DOE/ER/60773--1

DE90 008657

Second Semi-Annual Progress Report

FUNDAMENTAL QUANTITATIVE ANALYSIS OF MICROBIAL ACTIVITY IN AQUIFER BIORECLAMATION

Bruce E. Rittmann and Albert J. Valocchi
Co-Principal Investigators
Department of Civil Engineering
University of Illinois at Urbana-Champaign

Philippe Baveye
Subcontract Principal Investigator
Department of Agronomy
Cornell University

Sponsored by
U.S. Department of Energy
Office of Energy Research
Ecological Research Division

and

MODELING THE TRANSPORT OF BIOLOGICALLY AND CHEMICALLY REACTIVE SOLUTES IN A TWO-DIMENSIONAL, HETEROGENEOUS INTERMEDIATE SCALE SYSTEM

Bruce E. Rittmann and Albert J. Valocchi
Co-Principal Investigators

Sponsored by
Battelle Pacific Northwest Laboratory

Report on Progress from August 1989
through February 1990

MASTER

DISTRIBUTION OF THIS DOCUMENT IS UNLIMITED

DISCLAIMER

This report was prepared as an account of work sponsored by an agency of the United States Government. Neither the United States Government nor any agency thereof, nor any of their employees, makes any warranty, express or implied, or assumes any legal liability or responsibility for the accuracy, completeness, or usefulness of any information, apparatus, product, or process disclosed, or represents that its use would not infringe privately owned rights. Reference herein to any specific commercial product, process, or service by trade name, trademark, manufacturer, or otherwise does not necessarily constitute or imply its endorsement, recommendation, or favoring by the United States Government or any agency thereof. The views and opinions of authors expressed herein do not necessarily state or reflect those of the United States Government or any agency thereof.

DISCLAIMER

Portions of this document may be illegible in electronic image products. Images are produced from the best available original document.

1. BACKGROUND

This grant was awarded officially by DOE in March 1989. The primary awardee is the Department of Civil Engineering at the University of Illinois at Urbana-Champaign; a subcontract is to the Department of Agronomy at Cornell University. The principal investigators at the University of Illinois are Bruce E. Rittmann and Albert J. Valocchi. The principal investigator at Cornell University is Philippe Baveye.

The University of Illinois also has a closely coupled subcontract, entitled "Modeling the Transport of Biologically and Chemically Reactive Solutes in a Two-Dimensional, Heterogeneous Intermediate Scale Experimental System," from Battelle Pacific Northwest Laboratory (PNL). Progress of the DOE and PNL projects is reported herein.

The project's reporting structure contains two types of reports. The first type is a quarterly internal progress report. The purpose of the internal reports is to keep all members of the research team abreast with developments in each area. The second type is a semi-annual report that is transmitted to DOE and PNL. Its main purpose is to inform the project sponsors of the research-team's progress and plans. This report is the second semi-annual progress report.

The project has four primary areas: (1) biodegradation of poorly soluble organic contaminants, (2) dual-limitation kinetics of electron donors and acceptors, (3) two-dimensional modeling of biofilm reactions in nonhomogeneous porous media, and (4) biologically induced clogging in porous media. Progress and plans for each are described below.

2. BIODEGRADATION OF POORLY SOLUBLE ORGANIC CONTAMINANTS

The key goal of this portion of the project is to investigate fundamental mechanisms controlling in-situ biodegradation of nonaqueous-phase liquids (NAPLs) in porous media. The P.I. is B.E. Rittmann, and the research assistant is Eric Seagren.

Previous Accomplishments

During the first six months, the research emphasized the choice of organic compounds, the mass-transport mechanisms controlling biodegradation of NAPLs, and the choice of microorganisms.

Two compounds, decane and toluene, were selected for initial experimental work. Both are biodegradable under aerobic conditions, but toluene represents a NAPL with relatively high water solubility (515 mg/ℓ), while decane has very low water solubility (0.009 mg/ℓ 0).

Based on fermenter studies, three mass-transfer pathways were identified: uptake through direct contact of a large hydrocarbon drop and a surface-associated cell, uptake through direct contact of a sub-micron droplet and a cell, and uptake of NAPL molecules dissolved in the liquid. Extrapolation of fermenter results to a porous medium suggests that the first two mechanisms are most likely for very low-solubility NAPLs, while the third mechanism is most likely for the more soluble NAPLs.

Two potentially useful strains of Pseudomonas putida were obtained. One strain contains the OCT plasmid and grows on decane. The other contains the TOL plasmid and grows on toluene.

Progress

Dissolution Modeling

A major effort was placed on developing a mathematical model for biodegradation in a saturated porous medium containing lenses of NAPL. Such a

situation is one of the most important ones in subsurface bioremediation and can be evaluated experimentally in the laboratory with a column reactor that has horizontal flow and NAPL pools at the top or bottom. A second major effort was placed on determining the biodegradation characteristics of the Pseudomonas species.

The differential equation used to mathematically describe the transport of dissolved reactive constituents in a saturated, isotropic porous medium is known as the advection-dispersion equation (Freeze and Cherry, 1979). The two-dimensional form of the advection-dispersion equation for homogeneous media with steady flow in the x-direction and dispersion in the x- and y- directions can be written as follows (Gillham and Cherry, 1982):

$$\frac{\partial C}{\partial t} = D_x \frac{\partial^2 C}{\partial x^2} + D_y \frac{\partial^2 C}{\partial y^2} - \bar{v}_x \frac{\partial C}{\partial x} - G \qquad (2.1)$$

where C = solute concentration, mass of solute per unit volume of solution (ML^{-3}); t = time (T); D_x, D_y = longitudinal and transverse dispersion coefficients, respectively (L^2T^{-1}); x = distance in direction of flow (L); y = distance perpendicular to flow (L); $\bar{v}_x$ = average linear velocity (LT^{-1}); and G = source-sink term, mass of solute per unit volume of solution per unit time ($ML^{-3}T^{-1}$). The reaction term, G, represents all of the chemical and biochemical processes that alter the concentration of the solute in the solution phase (Gillham and Cherry, 1982).

In the case of the transport of dissolved NAPL components, the relevant reaction processes include the adsorption of dissolved NAPL components to aquifer solids, dissolution of dissolved NAPL components from NAPL present as a separate phase, and biodegradation of NAPL. The processes of NAPL dissolution and NAPL biodegradation are discussed with respect to the transport of the dissolved fraction of a single-component NAPL. The adsorption of dissolved NAPL components

is not covered at this time.

For case of steady-state transverse diffusion of NAPL from a pool into a semi-infinite medium, the advection-dispersion equation can be written as follows (Hunt et al., 1988, Fried et al., 1979):

$$\bar{v}_x \frac{\partial C}{\partial x} = D_y \frac{\partial^2 C}{\partial y^2} \quad \text{for } x, y > 0 \tag{2.2}$$

According to Gillham and Cherry (1982), the transverse dispersion coefficient, D_y, can be defined as follows:

$$D_y = D_d + D_m = D_o \tau + \alpha_y |\bar{v}_x|^n \tag{2.3}$$

where D_d = effective diffusion coefficient, D_m = coefficient of hydrodynamic (mechanical) dispersion, D_o = diffusion coefficient in free solution, τ = tortuosity, α_y = transverse dispersivity, and n = empirical constant (equal to or close to 1.0).

The boundary conditions for this problem are (Hunt et al., 1988; Fried et al., 1979):

(1) $C(x, y=\infty) = 0$ (2.4)

(2) $C(0 \leq x \leq L, y=0) = C_s$ = water solubility of chemical if pure substance

(3) $C(x=0, y) = 0$

where L = length of contaminant pool in x direction.

The solution to partial-differential equation (2.2), subject to the above boundary conditions, is (Hunt et al., 1988; Fried et al., 1979):

$$\frac{C(x,y)}{C_s} = \text{erfc}\left(\frac{y}{2} \sqrt{\frac{v_x}{D_y x}} \right) \tag{2.5}$$

where erfc = complimentary error function. The solution to equation (2.5) for a pool of pure n-decane and using the values in Table 1 is presented in Figure 1. The results for toluene would be very similar, since the dispersion

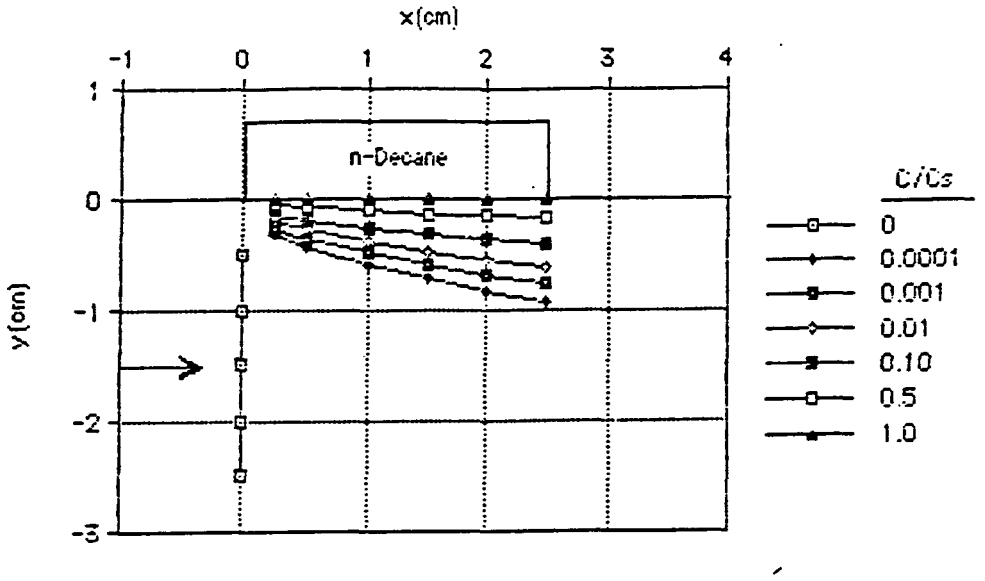

Figure 1. Steady-state transverse diffusion of n-decane from a pool into a semi-indefinite medium.

Table 1. Values used to solve equation (2.5).

q	= 100 cm/day
η	= 0.40
$\bar{v}_x$	= 250 cm/day
$D_{o\ n\text{-decane}}$	= 6.06×10^{-6} cm^2/s (calculated using Wilke Chang equation (Welty et al., 1984))
τ	= 0.67
α	= 0.01 cm
D_d	= 4.06×10^{-6} cm^2/s
D_y	= 2.85 cm^2/day
L	= 2.5 cm

coefficients are of the same order of magnitude.

The analysis predicts that the concentration of n-decane at the end of the contaminant pool is significantly less than the solubility limit of n-decane in water. The average concentration and, in turn, the average fraction of the

water solubility in the aquifer at the end of the contaminant pool can be calculated as (Hunt et al., 1988):

$$\bar{C}(L) = \frac{1}{Y}\int_0^Y C(L,y)\,dy \qquad (2.6)$$

and

$$\frac{\bar{C}(L)}{C} = \frac{1 - e^{-\omega^2}}{\omega\sqrt{\pi}} \qquad (2.7)$$

where Y = thickness of aquifer and

$$\omega = \frac{Y}{2}\sqrt{\frac{\bar{v}_x}{D_y L}}$$

Using Y = 2.5 cm makes $\bar{C}(L)/C_s = 0.076$, which for n-decane (water solubility = 0.009 mg/L at 20°C (Vershueren, 1983)) translates into an average concentration at the end of the pool of 0.7 μg/L. Under these conditions, it would take an extremely long time to remove the NAPL present as a pool with just pumping.

The next step is to adapt the two-dimensional model, described under section 4 of this report, to the situation in which a NAPL pool is present at the top or bottom of the porous medium. This numerical model will be used directly to evaluate different reactor configurations to be used for laboratory experiments on NAPL dissolution, transport, and biodegradation. Besides being useful for reactor design the two-dimensional model will be used to evaluate the results of experiments in which biodegradation and dissolution from the NAPL occur simultaneously.

Biodegradation

In order to model the degradation of components of a NAPL, it is necessary to determine which mass-transfer pathway is utilized for hydrocarbon uptake. A series of experiments was performed to begin the characterization.

To begin, P. putida PpG6 (the decane oxidizer) was grown in batch shaker-flask cultures with n-decane as the sole carbon and energy source. The growth

experiments were carried out in 500-ml side-arm flasks containing 100 ml of autoclaved mineral Medium B (Claus and Walker, 1964). The Medium B was inoculated with 1 ml of aqueous phase from another liquid culture of PpG6, also grown on decane. Then, 10 ml of n-decane was layered on top of the Medium B by injecting it from a syringe through an autoclaved Acrodisc 13CR (0.2 micron) disposable filter unit, the flasks were then placed on a wrist-action shaker water bath at 30°C. Growth was measured by determining the absorbance of the aqueous phase in a Bausch and Lomb Spectronic 20 using a wavelength of 660 nm and autoclaved Medium B as the blank. Figure 2 is a typical result. During these experiments, cells were microscopically observed to be on the surface of drops of n-decane; therefore, the absorbance measurement provides only an estimate of the changes in cell mass, since cells were also in the hydrocarbon phase.

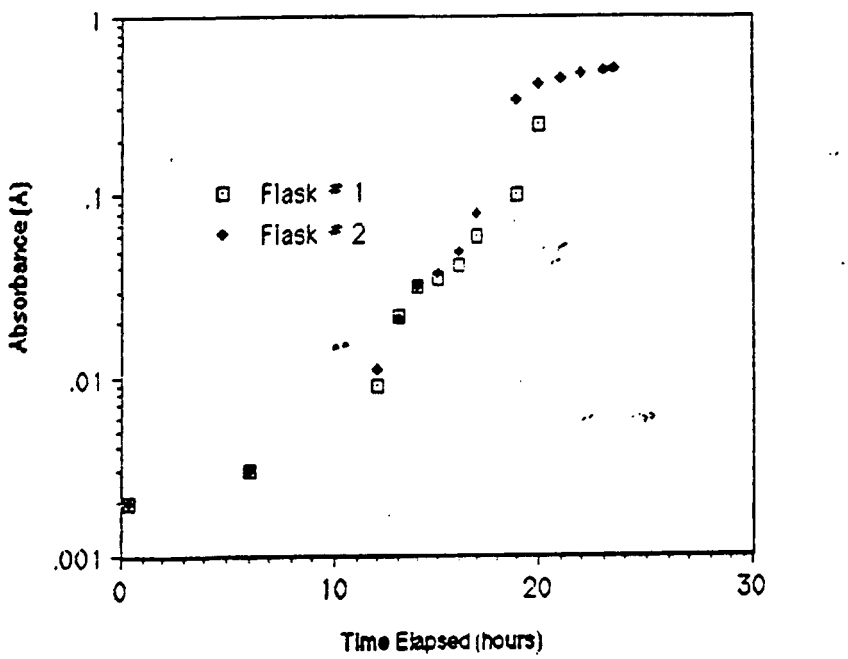

Figure 2. Growth curve for Pseudomonas putida PpG6 with n-decane as carbon and energy source.

The growth-curve tests were performed in a modified manner to gain more detailed insight into the relative importance of growth in the aqueous phase and on the decane phase. Fourteen 250-mℓ Erlenmeyer flasks containing 50 mℓ of autoclaved Medium B were each inoculated with 0.5 mℓ of broth from a previous growth experiment. Periodically, one flask was sacrificed, and the cells were killed with addition of 0.25 mℓ Formalin (i.e., 37% formaldehyde)(Mallette, 1969). The sample was poured through a funnel into a separatory funnel, and the phases separated almost immediately. The aqueous phase was drained slowly and vacuum filtered through a 0.2-um Nucleopore PC Membrane filter that had been prepared previously by washing with distilled water and drying to constant weight at 105°C. When all of the aqueous phase had been filtered, the filter was washed with a small volume of distilled water. Next, the decane phase was drained and vacuum filtered through another prepared membrane filter. The funnel and separatory funnel were rinsed with 1% aqueous Tween 20 to wash down droplets adhering to the glass. When the decane had been completely filtered, the filter was washed with 1% aqueous Tween 20. All membrane filters were dried at 105°C and reweighed to give dry weight.

The results are summarized in Figure 3. Initially and for the first 12 hours, more cell mass was associated with the decane phase, and growth is not evident; however, because dry weights were near the limit of detection, growth could not be observed reliably near the beginning of the tests. After 12 hours, growth was steady for the decane-associated cells, with a first-order rate of increase of approximately 0.15/hour, or 3.7/day. For the aqueous phase, experiment 1 gave more reasonable results and is discussed. The increase was roughly first order, with a rate of approximately 0.21/hour, or 5.2/day. Because of the faster increase in the aqueous phase, the dry weights were nearly equal

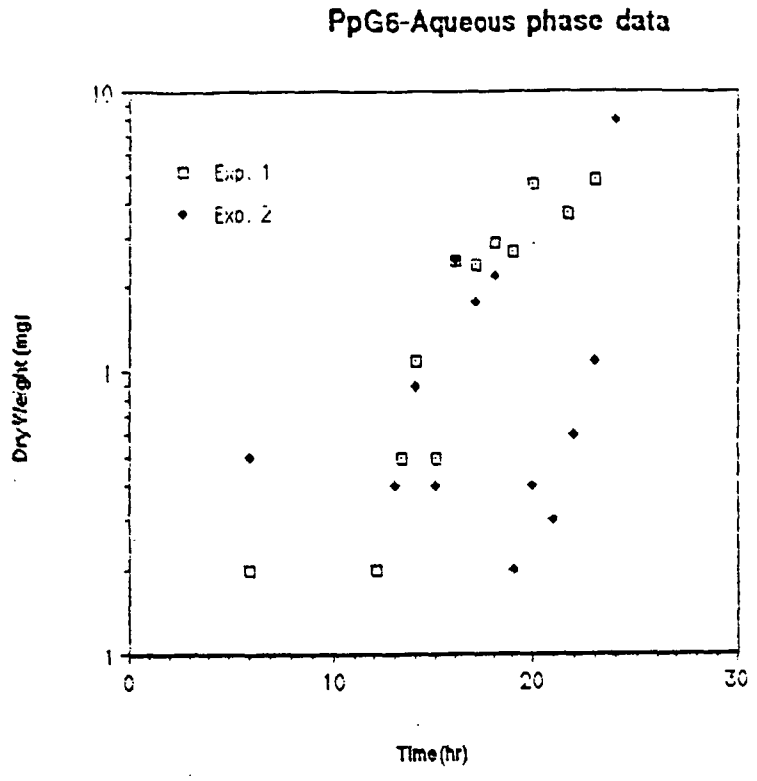

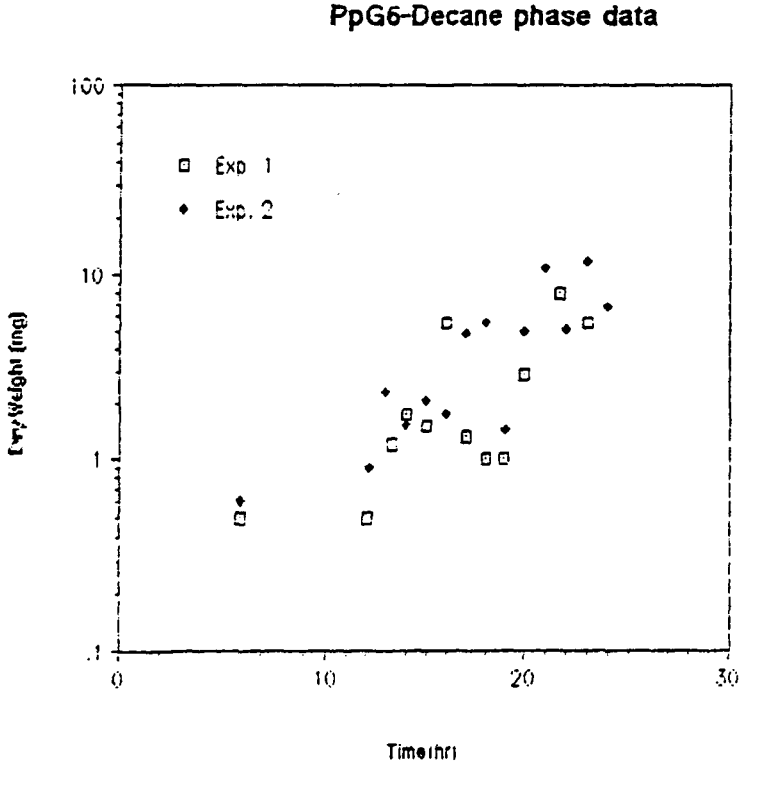

Figure 3. Results for the suspended dry weight in the aqueous phase (top) decane and phase (bottom) for two growth experiments with P.putida PpG6.

by 24 hours.

The results of Figure 3 show clearly that the majority of the cell mass and its increase was associated with the decane phase. While not absolutely conclusive, these data suggest strongly that P. putida PpG6 is not inhibited by decane. In addition, it seems to grow directly on the decane surface.

Samples of the aqueous phase in these experiments were used to perform the Bacterial Adhesion to Hydrocarbon (BATH) test of Rosenberg et al. (1980). In this procedure, varying amounts of test hydrocarbon are added to test tubes containing washed cells suspended in a buffer solution. The mixture is agitated and then allowed to stand, allowing phase separation. The decrease in absorbance of the aqueous phase is used as a measure of the bacteria adhering to the hydrocarbon. The BATH results using 1 mL of n-decane as the test hydrocarbon are illustrated in Figure 4. Adherence of PpG6 changed with cell age and growth media. The cells grown with nutrient broth as the carbon and energy source were

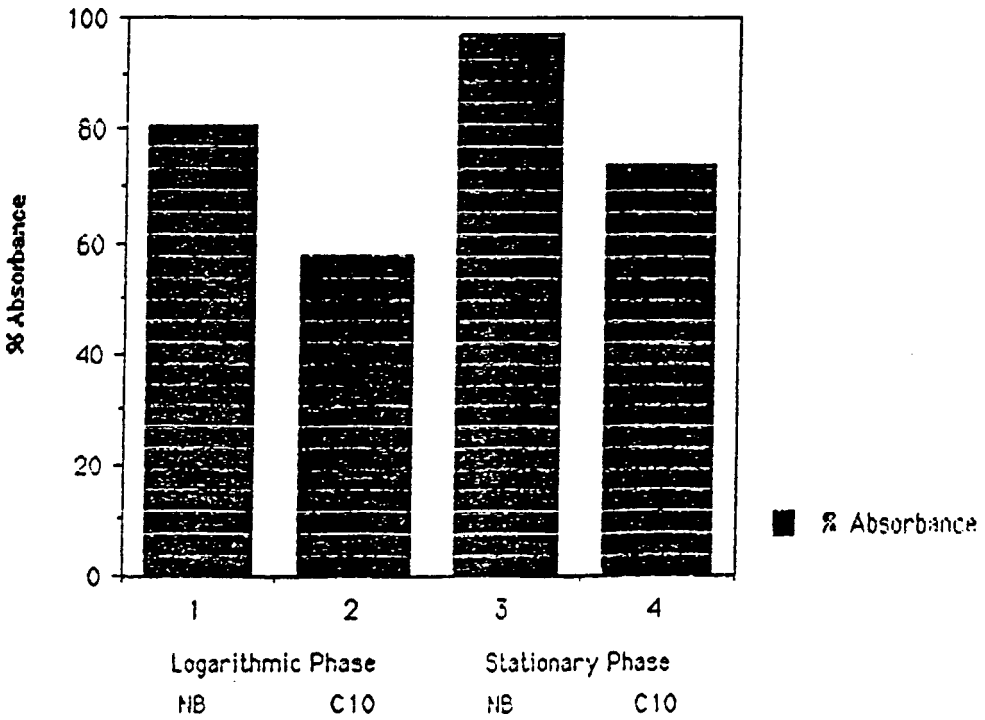

Figure 4. BATH results for Pseudomonas putida PpG6 grown on nutrient broth (NB) and n-decane (C10).

grown under the same mixing and temperature conditions as those grown on n-decane, and the growth followed by measuring absorbance. PpG6 showed little tendency to absorb to n-decane when grown on nutrient broth in the logarithmic-phase or the stationary phases; however, PpG6 cells grown on n-decane showed the highest level of adherence in the logarithmic phase. The results using 1 mL of n-dodecane as the test hydrocarbon were very similar; however, when 1 mL of toluene was used as the test hydrocarbon, high adhesion was exhibited by logarithmic-phase cells grown on nutrient broth and n-decane, while lower adhesion was exhibited by stationary phase cells.

Two experiments were performed to elucidate how P. putida PpG6 grows on toluene. In the first experiment, an inoculum previously grown on toluene was placed in a 250-mℓ Erlenmeyer flask containing 50 mℓ of autoclaved Medium B. In two flasks, 5 mℓ of toluene (10% v/v) was layered onto the Medium B. In two other flasks, 0.2 mℓ of toluene was placed in a glass tube that had a cotton plug which was immersed in the medium. The flasks were placed in a wrist-action shaker water bath at 30°C.

The flasks with 10% v/v toluene showed no turbidity. On the other hand, the flasks fed toluene that had to diffuse through the cotton plug showed turbidity and flocs. These results show that toluene present at its saturation concentration was toxic to P.putida, but that diffusion away from a point source gave enough decrease in toluene concentration to allow good growth.

A second experiment was performed in the same manner, except that direct addition of toluene was at 10%, 5%, and 1% v/v. Again, only the flask exposed to toluene diffusing from the point source supported growth. Therefore, toluene acts as a self-inhibitory substrate. It should be modelable with Haldane kinetics (Saez and Rittmann, 1989), which can be incorporated into the two-

dimensional model.

Future Directions

Future work on biodegradation will focus on further elucidation of how P. putida PpG6 grows on decane, refinements to the experiments measuring growth on decane, developing a model of P.putida's utilization of dissolved and separate-phase decane, and quantifying the Haldane kinetics for toluene.

3. DUAL-LIMITATION KINETICS

Dual limitation refers to a situation in which the electron donor and electron acceptor limit the overall cell-growth rate together. The P.I. for this portion of the research is B.E. Rittmann, and the research assistant is Wookeun Bae. Dual limitation can take place most frequently in in-situ bioreclamation when an electron donor is the contaminant and an electron acceptor is injected. Once a dual-limitation condition develops, the cell-growth rate and the substrate utilization rate become lower than predicted from single limitation by either substrate.

Previous Accomplishments

A literature review revealed that bacteria respond to decreases in electron donor or electron acceptor by altering their concentrations of internal substrates. Under electron-donor depletion, the NAD/NADH ratio increases (Matin and Gottschal, 1976), while the NAD/NADH and ATP/ADP ratios decrease under electron-acceptor depletion (Harrison et al., 1969; Wilson et al., 1977). A structured kinetic model was presented in the first semi-annual progress report. The model expresses the overall rate of substrate utilization as a function of the concentrations of each substrate, stoichiometry, and response factors for NAD/NADH and ATP/ADP.

An experimental program utilizing chemostats was described. The specific growth rate and concentrations of acetate and O_2 are varied. Two Pseudomonas putida strains, PpF1 and PpG9, were selected for initial experimentation. Because PpF1 gave a higher maximum specific growth rate and a higher true yield, it was selected for further experiments.

Porous-medium experiments with biofilms also were described. They are designed to demonstrate the decrease in substrate flux as dual limitation occurs.

Progress

A major effort was placed on development of analytical techniques capable of accurately measuring intracellular concentrations of NAD, NADH, ATP, ADP, and inorganic orthophosphate P. As the concentrations of these internal substrates are low and might change quickly, very sensitive techniques are required. Because standardized methods are not available in each case, suitable methods were developed by modifying or combining techniques originally developed for other purposes.

NAD and NADH

Since NAD and NADH concentrations in bacterial culture usually are less than 1 μM), the conventional spectrophotometric-absorption method (sensitivity c. 200 μM) is inadequate. Consequently, a highly sensitive cycling method that combines alternate reduction and oxidation of NAD(H) and production of fluorescence was developed. Figure 5 illustrates the concept.

NAD is reduced to NADH in the presence of ethanol and alcohol dehydrogenase. NADH, in turn, reduces phenazone methosulfate (PMS) to its reduced form ($PMS \cdot H_2$), which finally reduces resazurin to its fluorescent product resorufin. Since the reduction and oxidation of NAD(H) is cyclic, the resorufin is produced continuously until ethanol or resazurin is exhausted; the rate of resorufin formation is proportional to the concentration of NAD or NADH.

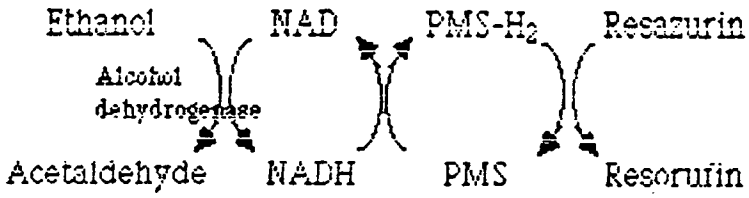

Figure 5. Cycling reaction of NAD(H) and fluorescent resorufin production.

The rate of resorufin formation can be detected in a fluorescence spectrophotometer. The fluorescence is an emission of radiant energy from a substance which has been excited by absorption of visible or UV radiation. Since the fluorescent radiant energy is proportional to the exciting radiant energy, as well as to the fluorescent substrate concentration, the sensitivity can be increased by increasing the exciting energy, which is a major advantage over absorption spectrophotometry, in which the sensitivity is solely determined by the amount of absorption. Determination of NAD and NADH is done in two steps: extraction from the cells and enzymic assay/instrumental detection. The following method is modified from Matin and Gottschal's method (1976), which was originally advanced by Cartier (1968) and Wimpenny and Firth (1972).

Extraction. 3-mL aliquots of steady-state culture were added into test tubes that contained 0.5 mL of 0.75 N HCl (for NAD extraction) or 0.75 N NaOH (for NADH extraction). In acid, NAD is stable, but NADH is destroyed; thus, acidic extraction contained only NAD. On the other hand, NAD is destroyed in an alkaline solution, while NADH is stable; thus, alkaline extraction contained only NADH. After being thoroughly mixed, the tubes were incubated in a 50°C

water bath for 12 min. After incubation, the tubes were cooled to 0°C on ice and neutralized by slow addition (approximately 10 μL/min) of 0.5 mL of 0.75 N NaOH (for NAD extraction) or 0.75 N HCl (for NADH extraction), supplemented with Tris buffer (pH 7.6) to a final concentration of 0.11 M. It was observed that the neutralization step was very important: Improper mixing induced local high concentration of base or acid, resulting in loss of cofactor molecules, while inadequate neutralization (too high or too low pH) affected the subsequent enzymatic assay. The neutralized extract was centrifuged for 15 min at 4°C and assayed as quickly as possible. The extract was stored on ice until assay/detection.

Enzymatic Assay/Detection. The enzymatic assay is a procedure to produce fluorescent material, as depicted in Figure 5. The assay mixture contained (in μL) distilled water, 1000; Tris buffer (0.2 M, pH 7.6), 500; ethanol, 100; dipyridyl (0.1 g dipyridyl/100 mL ethanol, diluted 20 times with water before use), 100; resazurin (0.2 mM stock solution, diluted 10 times before use), 100; phenazone methosulfate (6 mg/L), 100; alcohol dehydrogenase (3000 units/mL frozen stock, diluted to 500 units/mL before use), 25; sample extract or standard, 100. Since the reaction rate was also dependent on the concentrations of phenazone methosulfate and alcohol dehydrogenase, keeping exact concentration of reagents was very important.

Two precautions in choosing chemicals were necessary to ensure satisfactory measurement. First, most commercial sources of resazurin contained a significant amount of resorufin as an impurity, resulting in high background fluorescence. This background fluorescence caused the measurement to be very inaccurate. Only one product (Aldrich, 99% in purity) gave a satisfactory result. Second, certain alcohol dehydrogenase contained enzyme-bound NAD and NADH, also giving high background fluorescence formation. A product from Sigma chemicals (A 3263) was

acceptable.

A fluorescence spectrophotometer (Perkin-Elmer, Model MPF-44B) was used to measure the resorufin formation. Optimum excitation and emission wavelengths were 573 and 585 nm, respectively. This was slightly different value from those reported by Cartier (1968).

Measurements with chemostat cultures gave satisfactory results. The concentrations of NAD and NADH in an electron-donor limited chemostat culture fell in the range of reported values. Standard extractions gave good linearity between concentration and the rate of fluorescence formation.

ATP and ADP Measurement

Principle. ATP that reacts with firefly luciferin in the presence of luciferase produces bioluminescence through formation of enzyme-bound luciferyl adenylate. The luminescence is proportional to the ATP concentration, as shown here:

$$ATP + LH_2 + 1/2\ O_2 \xrightarrow{\text{firefly luciferase}} L^{\circ}AMP + PP_i + H_2O + \text{light}$$

$$ADP + PEP \xrightarrow{\text{pyruvate kinase}} ATP + \text{Pyruvate}$$

This bioluminescence can be quantified by using a spectrophotometer or a scintillation counter. ADP can be determined when it is enzymatically converted to ATP in the presence of phosphoenolpyruvate and pyruvate kinase. Critical steps in ATP measurement are the extraction of ATP from the cells and the detection of the luminescent energy produced. In the case of ADP, enzymatic conversion of ADP to ATP also is essential. The following methods were based on the methods by Holm-Hansen and Karl (1978) and Cheer et al. (1974).

Extraction. 0.1 mL of chemostat culture was quickly transferred into 5 mL of boiling Tris buffer (20 mM, pH 7.75) in a scintillation vial. The vial was capped, and the liquid boiled for 5 minutes. The boiling buffer quickly denatured the thermolabile ATPase and simultaneously extracted ATP and ADP from

the cells. The extract was cooled and assayed immediately.

ADP Conversion. 400 mL of extract or standard was added into each of two glass culture tubes, denoted A and B. Addition of 50 μL of a solution containing $MgCl_2$(15 mM), potassium phosphate buffer (75 mM pH 7.4), phosphoenol pyruvate (0.5 mM, tube B only), and 20 μg of pyruvate kinase (tube B only) followed. Tube B was incubated in a 30°C water bath for 30 minutes and then placed in 100°C boiling water for 2 minutes to stop the enzymic reaction. This tube contained ATP molecules originally existing and those converted from ADP. The fraction of ATP originally existing was determined by incubating the extract or standard without adding phosphoenol pyruvate and pyruvate kinase (tube A). The difference (ATP in tube B subtracted by ATP in tube A) was equivalent to ADP.

Assay for luminescence production and detection. The luciferin-luciferase system was prepared from crude firefly lantern extract (50 mg) by mixing 5 mL of distilled water, 10 mL of sodium arsenate buffer (100 mM, pH 7.4), and 10 mL of MgSO4 (40 nM). The mixture was aged for 3-4 hours at room temperature and filtered. 0.5 mL of the filtered luciferin-luciferase preparation was transferred into a counting vial (mini scintillation vial); then, 0.1 ml of sample was added. The luminescence production was measured in a scintillation counter for 30 seconds using a single-photon-count mode.

Two aspects were very important in ATP determination. First, the light emission reached the peak right after mixing the enzyme preparation and the ATP sample; the light emission diminished to a background emission with time. Therefore, immediate initiation of the counting was crucial to have reproducible results. Second, the degree of mixing or agitation affected counting, because undue shaking caused light emission. Therefore, a constant degree of mixing was also critical. Consequently, combining of proper mixing and prompt counting became a key factor for adequate measurement of ATP.

To meet the requirement of proper mixing and prompt counting, a semi-automatic injection/mixing system was developed. The system consisted of a pipet holder which held and aligned an automatic pipet tip (0.1 mL) right above the counting chamber in the scintillation counter and a 0.1 mL automatic pipet. The ATP sample was injected into a counting vial that contained the enzyme preparation just before the vial descended in the elevator toward the counting chamber. The system gave very satisfactory results.

Reproducible counting of ATP and ADP could be obtained with the chemostat culture. The standard curve gave linear relationship between concentration and counting.

Inorganic Orthophosphate (P_i) Measurement

Principle. P_i can be measured with a spectrophotometer after chemical color development. The most sensitive methods are based on the complex formation of phosphomolybdate at low pH with basic dyes, such as malachite green. The color-development procedure is relatively simple compared to enzymatic measurements. Separation of cells from a medium that contains very high concentration of P_i complicates the measurement, however.

Separation of the Cells and P_i Extraction. 2 mL of bacterial culture was filtered through a double layer (two sheets) of 0.45-μm filter papers. 20 mL of Tris buffer (2 mM, pH 7.2) was passed through to rinse the paper. The filtering and rinsing were completed within about 30 seconds to minimize potential increase of P_i in the cell by ATP hydrolysis or loss of P_i by cell lysis. The top and bottom filters were transferred to 5 mL boiling Tris buffer to extract them in a manner similar to the extraction of ATP. The bottom filter paper was used as a blank, since a small amount of P_i adhered and remained even after rinsing.

Color Development and Measurement. Color development was based on the ultrasensitive P_i detection method advanced by Hess and Derr (1975) and subsequently improved by Lanzetta et al. (1979). A color reagent was prepared by preparing a 3:1 mixture of 0.045% malachite green hydrochloride (MG) and 4.2% ammonium molybdate in 4 N HCl (AM). The mixture was agitated for 30 minutes and filtered (MG/AM). 1 mL of 1% Sterox (detergent) was added to 25 mL of MG/AM solution.

Color was developed by adding 0.5 mL of sample or standard into 4 mL of the reagent mixture. After mixing and waiting for 1 minute, 0.5 mL of 34% (w/v) sodium citrate dihydrate solution was added and mixed. After allowing 30 minutes for full color development, the color intensity was measured with a spectrophotometer of 660 nm.

P_i measurements with chemostat cultures gave reproducible results, and a standard run showed good linearity between absorption and concentration.

Chemostat Experiments

The analytical techniques were applied to a series of chemostat experiments in which the electron donor (acetate) was the rate-limiting substrate. Acetate was fed at a concentration of 1000 mg COD/ℓ for all runs. The electron acceptor (O_2) and all nutrients were supplied at non-limiting levels.

Four experimental runs were completed so far. The dilution rate was varied from 0.05 μ_m to 9.7 μ_m, where μ_m is the cells' maximum specific growth rate, about 0.5/hour (12/day). Concentrations of cell dry weight, soluble organic carbon, inorganic P, and all intracellular co-factors were assayed at steady state.

The results are summarized in Table 2. The two columns for run R8 occurred because the initial steady state was unstable and gave way to a second steady state, which was comprehensively analyzed.

Table 2. Steady-state concentrations of external and internal substrates in chemostat experiments.

Run Designation	R6	R1	R5	R8-I	R8-II
Dilution Rate, hr^{-1}	0.03	0.06	0.24	0.38	0.38
Cell Dry Weight, mg/ℓ	151	157	162	105	166
SOC, total, mg COD/ℓ	8.3	3.5	7.3	173	6.9
SOC<500 daltons, mg COD/ℓ	1.1	0.9	1.1	---	---
NAD, μmole/g cells	3.75	4.1	3.8	---	3.5
NADH, μmole/g cells	0.032	0.11	0.15	---	0.075
NAD/NADH	117	37	26	---	45
ATP, μmole/g cells	16.4	14.1	13.1	---	10.6
ADP, μmole/g cells	4.6	4.8	3.8	---	2.3
ATP/ADP	3.5	2.9	3.4	---	2.3
P_i, μmole/g cells	45	21	15 to 46	---	71

Except for R8-I, the acetate was nearly completely utilized. The acetate concentrations were below the detection limit of gas chromatography (0.5 mg COD/ℓ). Most of the COD in the effluent was soluble microbial products. If acetate concentration is to be measured in acetate-limiting chemostats, a more sensitive analytical technique is needed.

NAD concentrations in the cells did not change much as the dilution rate was varied. On the other hand, NADH concentrations rose significantly as the dilution rate increased. except for R8, the NAD/NADH ratio increased as the cells grew faster and (presumably) were exposed to a higher acetate concentration. This observation is parallel to that of Matin and Gottschel (1976) and is what we anticipated. With the electron donor being more available, the reduced form of the internal electron carrier (i.e., NADH) should increase.

ATP and ADP concentrations decreased somewhat as the dilution rate increased, but the ATP/ADP ratio remained nearly constant. Again, a relatively constant ATP/ADP ratio was expected for changes in dilution rate when the electron donor limits alone.

There was no obvious trend in the inorganic P_i concentrations within the cells. Part of the variability may be caused by a high P concentration in the

liquid medium. Any residual liquid associated with the cells could alter the measured concentration of internal P. Nonetheless, the lack of any major trend in P_i is consistent with our expectations.

In summary the steady state data confirm that measurement of internal concentrations of NAD, NADH, ATP, and ADP are adequate. Furthermore, the trends in NAD/NADH and ATP/ADP conform to our expectations.

Future Directions

One major effort will focus on transient-state experiments to measure how the acetate utilization rate depends on NAD/NADH and on ATP/ADP. A second major effort will investigate electron-acceptor (O_2) limitation and how it affects NAD/NADH and ATP/ADP.

4. TWO-DIMENSIONAL MODELING

The principal investigator for the two-dimensional modeling of nonhomogeneous aquifers containing microbial activity and sorbing substrates is A.J. Valocchi. The research assistant is Joseph Odencrantz. The work on the 2-D modeling is funded separately by a grant from Battelle Pacific Northwest Laboratory, but is closely coordinated with the DOE-supported research.

Previous Accomplishments

The First Semi-Annual Progress Report described two alternate numerical models we have implemented for solving the two-dimensional advection-diffusion-reaction equations. Most of our work so far has considered the simultaneous transport of an organic electron donor and an electron acceptor subject to dual-Monod biodegradation kinetics. In this case, the governing mass balance equation for the electron donor is

$$\frac{\partial S}{\partial t} = - v_i \frac{\partial S}{\partial x_i} + \frac{\partial}{\partial x_i} D_{ij} \frac{\partial S}{\partial x_j} - R_S ; \quad i,j = 1,2 \qquad (4.1)$$

where

$$R_S = M_t \, q_m \left(\frac{S}{K_s + S}\right)\left(\frac{A}{K_A + A}\right) \tag{4.2}$$

and

M_t = total active microbial mass concentration

q_m = maximum rate of substrate utilization

S and A = mass concentration of organic compound and electron acceptor

K_s and K_A = half velocity constant of organic compound and electron acceptor

v_i = average linear velocity vector

D_{ij} = hydrodynamic dispersion coefficient

R_S = biodegradation term

There are analogous mass balance equations for the electron acceptor (A) and the biomass (M_t).

The first numerical model we have implemented is the Principal Direction Finite Element Method (PDFEM) of MacQuarrie et al. (1989). The PDFEM is structured as an alternating direction solution algorithm; the nonlinear coupling caused by the biodegradation term (4.2) is handled by standard iteration. The second model we have implemented is an operator-splitting (OS) method which decouples the reaction term from the advection and dispersion terms (Wheeler, 1988; Wheeler and Dawson, 1987). Operator-splitting essentially breaks equation (4.1) into

$$\frac{\partial S}{\partial t} = - v_i \frac{\partial S}{\partial x_i} + \frac{\partial}{\partial x_i} D_{ij} \frac{\partial S}{\partial x_j} \tag{4.3}$$

$$\frac{\partial S}{\partial t} = - R_s \tag{4.4}$$

where equation (4.3) is solved by the nonreactive PDFEM and equation (4.4) is solved by an ordinary differential equation solver. Details about the integration of (4.3) and (4.4) over a time step are provided in the First Semi-Annual Progress Report. Although we suspect OS to be more computationally

efficient than PDFEM, our main motivation for developing OS is the resulting modular structure of the numerical code. Alternative biodegradation submodels (or even submodels for other types of reactions such as adsorption) can easily be incorporated via modification of the right-hand-side of equation (4.4). On the other hand, modification of the PDFEM would be an elaborate and time-consuming endeavor.

Progress

General Performance of Operator-Splitting

In order to determine the performance of operator-splitting several criteria were considered. Recall from the First Semi-Annual Report that the advection-dispersion time step to solve (4.3) is divided into many smaller time steps for the reaction equation (4.4); a fourth-order Runge-Kutta method is used for (4.4). The first criteria was efficiency and was examined by comparing the operator-splitting execution time as a function of the number of Runge-Kutta steps to the standard PDFEM execution time, as discussed in the last progress report. The second criteria considered was accuracy, and the operator-splitting technique was again compared to PDFEM. Each of the criteria for performance has been evaluated and are discussed in greater detail in the next few paragraphs.

The timings of OS compared to the standard PDFEM are really the only way to get an idea of the efficiency between the two techniques when all three transport equations are solved simultaneously. The OS technique is noniterative and the execution time is a linear function of the number of Runge-Kutta steps taken. The standard PDFEM code does involve iteration and the execution time is a function of the desired error tolerance which controls the iteration. In order to demonstrate the efficiency of the operator-splitting technique, timings were done with the example problem from the First Semi-Annual Progress Report which involved a continuous partial-line source along the inflow boundary of a

domain with one-dimensional flow. The problem consisted of 231 computational nodes and the simulation was carried out for 10 days with a time step of 0.5 day, with grid Courant and Peclet numbers of 0.5 and 1.0, respectively. Figure 6 shows the execution time in cpu seconds for both operator-splitting and the standard PDFEM code as a function of the number of Runge-Kutta steps and tolerances, respectively. It can be observed from Figure 6 that the standard PDFEM at the highest tolerance and the noniterative solution of operator-splitting with no Runge-Kutta steps taken nearly the same time. This is essentially the case of solving three nonreactive transport equations (for S, A, and M_t) with PDFEM. The timings were done on an Apollo workstation Series 3500. The tolerance is actually a concentration value in micrograms per liter,

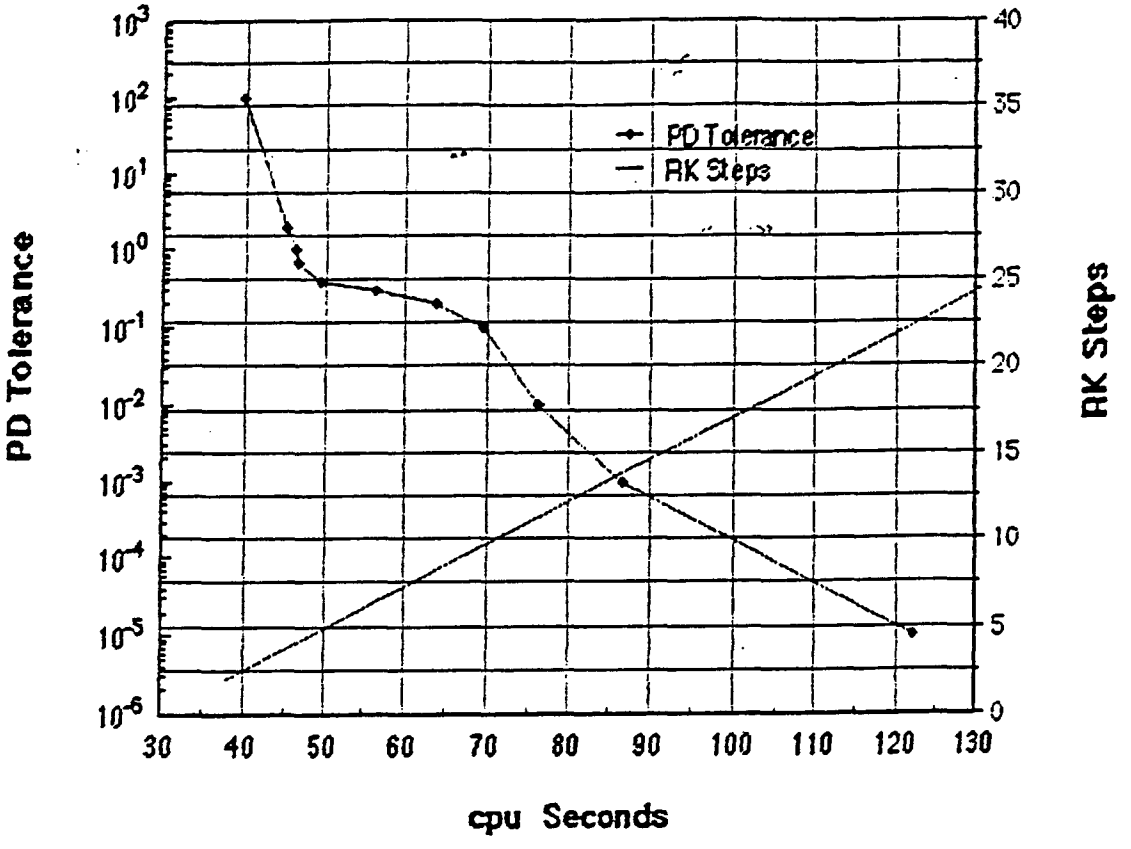

Figure 6. Comparison of execution times for the PDFEM and OS code solutions of the example problem.

and is defined as

$$\delta S_{max} < \eta$$

where $\delta S_{max} = \max|(S_j)_{i+1} - (S_j)_i|$, η = concentration tolerance, j = node, and i = iteration level.

The next performance criterion is accuracy. Accuracy is a very difficult property to measure since there are no analytical solutions available for the three coupled, nonlinear transport equations. The only approach that can be taken is to give the standard PDFEM code a very strict tolerance and use the solution as a basis for comparison. There is another alternative, and that would be to use only one noncoupled solute transport equation with either first or zero-order kinetics for which there is an analytical solution available. This approach is taken below; however, it lacks in being able to aid in the analysis of the coupled problem.

There are basically two problems which arise when considering the use of the standard PDFEM code as a basis for comparison. The first is which tolerance will be used to approximate the true solution and the second is a basis to compare the results of the operator-splitting technique. To best address these issues, the second problem should be considered first. A standard measure of error is necessary to compare the solution at each of the 231 nodes in our model problem. The relative sum of the squares is a standard means by which an analytical and numerical solution can be compared. The form of the equation which will yield the total relative sum of the squares for the computational grid at a particular time in the simulation is

$$RSS = \sum_{i=1}^{N} \left(\frac{S_{ai} - S_{Ni}}{S_{ai}} \right)^2 \qquad (4.5)$$

where S_{ai} is the value of the "analytical" solution at grid point i, S_{Ni} is the

value of the numerical solution at grid point i, and N is the total number of grid points in the computational domain.

The next problem to consider is what tolerance should be used for the standard PDFEM to best approximate the true (i.e., "analytical") solution. The approach was to choose a very small tolerance (8 orders of magnitude smaller than the injection concentration, e.g., 10^{-5} $\mu g/\ell$ for the organic compound) and examine the relative sum of squares (RSS) of larger tolerances compared to the solution at the very small tolerance. As the tolerances decreased from 10^{2} to 10^{-4}, so did the RSS. Therefore, the solution of the standard PDFEM code at the extremely small tolerance level was used as a basis for comparison. Further study should encompass two additional areas. Since we are not trying to suggest that the PDFEM solution with an error tolerance of 10^{-5} $\mu g/\ell$ is the true solution, perhaps further examination at an even lower tolerance would reveal a significant RSS when compared to the solution at a tolerance of 10^{-5} $\mu g/\ell$. A machine with a greater finite precision, such as the Cray 2, could aid in the solution of the problem. The other area to explore is that of true analytical solutions for the simplifying conditions as mentioned previously.

Figure 7 is a plot of the number of Runge-Kutta steps used in the operator-splitting routine versus the RSS, defined by (4.5) where S_a represents the standard PDFEM solution at the smallest error tolerance. All results are for our model problem at 10 days into the simulation. It is quite evident that the RSS decreases dramatically as the number of Runge-Kutta steps increases and converges to an extremely small RSS. Ideally the RSS should converge to zero if operator-splitting was to converge to the result obtained from the standard PDFEM. However, there are several potential reasons for the discrepancy between operator-splitting and the standard PDFEM. First, the time scale of advection and dispersion is assumed to be greater than that of biological reaction. There

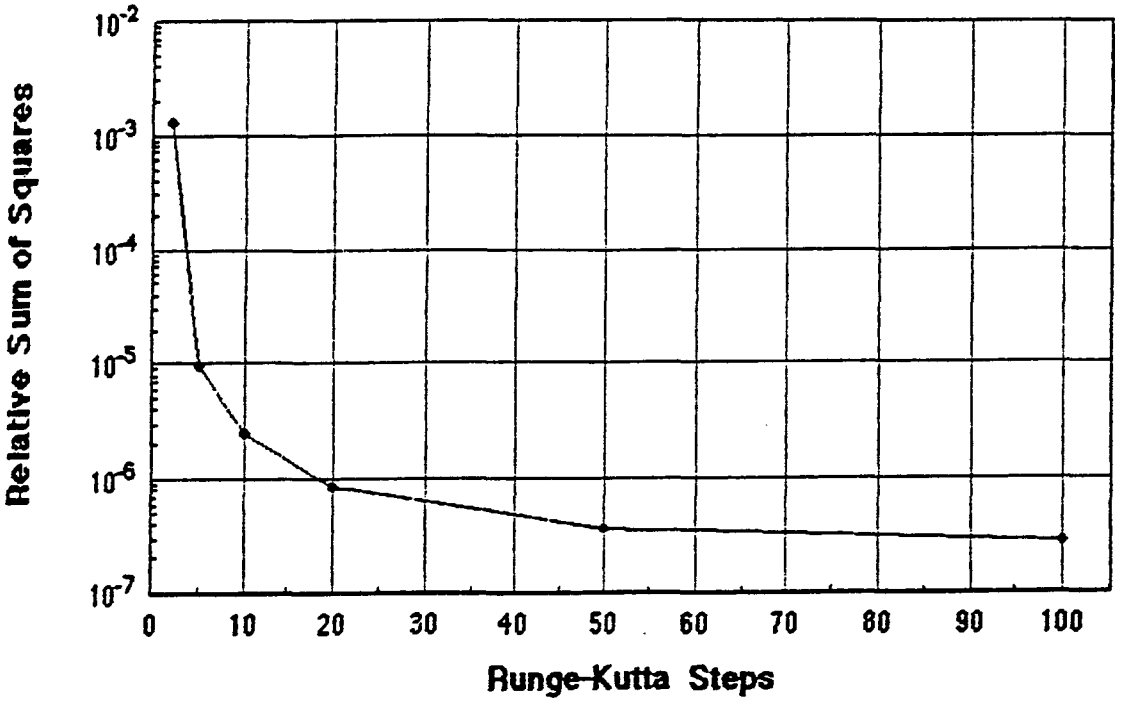

Figure 7. The relative sum of squares defined by equation 4.5 versus the number of Runge-Kutta steps used in the OS solution of the example problem.

may be a small amount of error inherent in the operator-splitting technique which is most probably dependent upon the time scale difference. This could be an important consideration that has not been addressed explicitly by previous researchers in their operator-splitting algorithms for similar problems of solute transport. A shorter time step than that required by the PDFEM Peclet and Courant criteria may be necessary to possibly alleviate the very small RSS difference. Second, the error may be attributable to the standard PDFEM not being the exact solution of the system of transport equation. Third, there may be a potential problem in that the output arrays that were used to calculate the RSS were formatted to only eight significant figures.

Operator-Splitting Compared to Analytical Solution in One Dimension

The operator-splitting model was compared to an exact anaylytical solution of a solute undergoing first-order decay. The system of equations (i.e., 4.1 and its equivalent for the electron acceptor) can be reduced to first-order for the organic compound (S) if $K_s >> S$, $A >> K_a$, and the microbial mass is held constant. The governing linear equation for this situation would be analogous to equation (4.1) with $R_s = \lambda S$, where $\lambda = M_t q_m / K_s$. The governing mass balance equation for the electron acceptor and biomass do not need to be solved because they are held constant. Figure 8 shows the boundary conditions and transport parameters used for the comparison. Also, $\Delta x = 0.5$ m and $\Delta t = 0.025$ d. In order to demonstrate the performance of operator-splitting, a wide range of first-order rate constants were chosen. The value of the rate constants are also shown in Figure 8 and vary over three orders of magnitude. The analytical solution is based on a semi-infinite domain in the direction of the flow; a free-exit boundary (Frind, 1988) is imposed for the node located along the outflow boundary

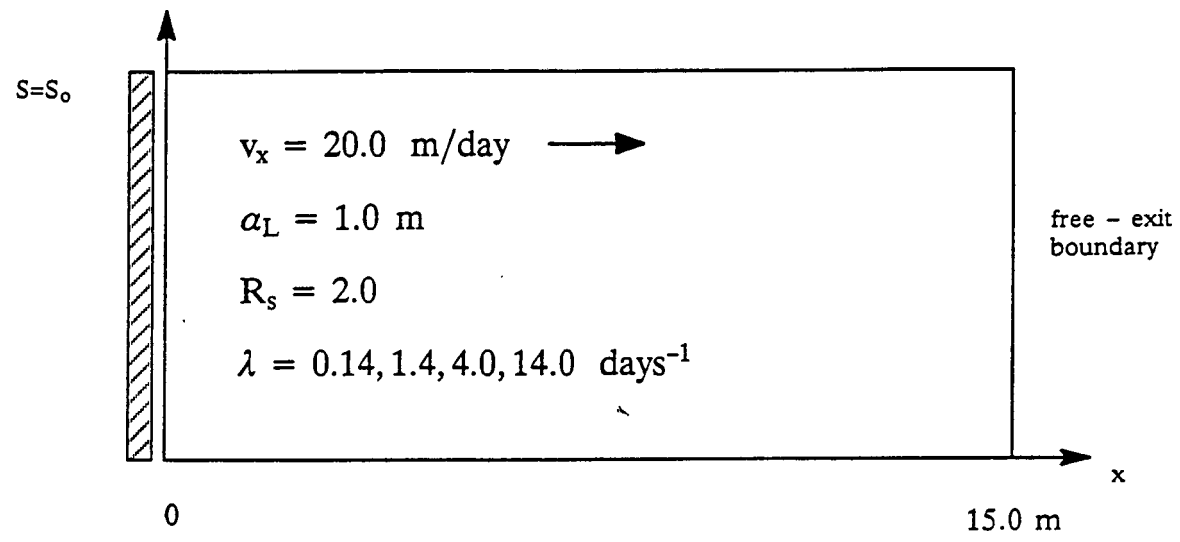

Figure 8. Boundary conditions and transport parameters for numerical and analytical comparison in one-dimension with several first-order kinetic constants.

in the PD finite element grid.

Figure 9 compares longitudinal profiles from the numerical and analytical solution for the different first-order rate constants at time 0.50 days. The leftmost curve closest to the origin is for the highest rate constant (λ = 14 days^{-1}). Ten Runge-Kutta steps per PD time step were used to solve for reaction term. In this case, an analytical solution could have been used to solve $dS/dt = -\lambda S$. However, Runge-Kutta was chosen for it will be the solution technique used in the general two-dimensional case with nonlinear reaction. The agreement between the two solutions is seen to be excellent and verifies that operator-splitting accurately simulates the processes of an advection, dispersion and first-order decay, even with large variations in the decay constant.

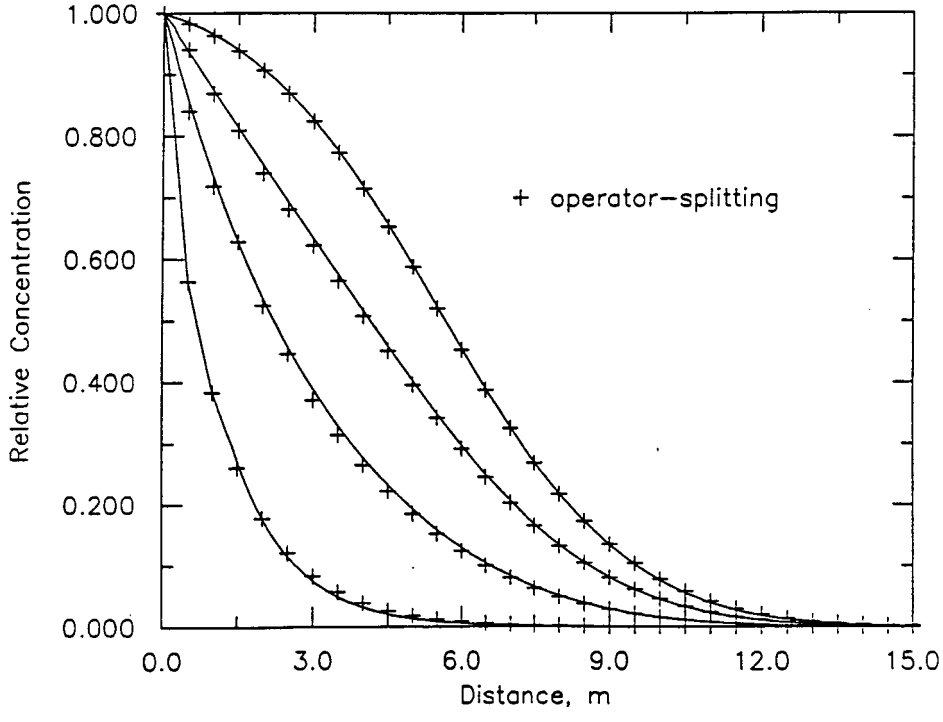

Figure 9. Analytical (solid lines) and numerical (symbols) solution comparison in one-dimension at time 0.50 days. The first order rate constants (days^{-1}) for each curve (going from left to right) are: 14.0, 4.0, 1.4, and 0.14.

Operator-Splitting Compared to Analytical Solution in Two Dimensions

The comparison in two dimensions was done with one first-order loss constant, and longitudinal and transverse profiles at selected times were compared. Figure 10 shows the location of the continuous source (first-type boundary), boundary conditions, and transport parameters used for the two-dimensional comparison. In this example, $\Delta x = 0.5$ m, $\Delta z = 0.125$ m, and $\Delta t = 10$ d. Once again, only the transport equation for the organic (S) with first-order loss needs to be solved. The two-dimensional nonreactive solute transport equation is solved using PD and then the concentration at every node is reacted using Runge-Kutta. Ten Runge-Kutta steps per PD time step were used. Realistic value of laboratory-scale longitudinal and transverse dispersivity were also used.

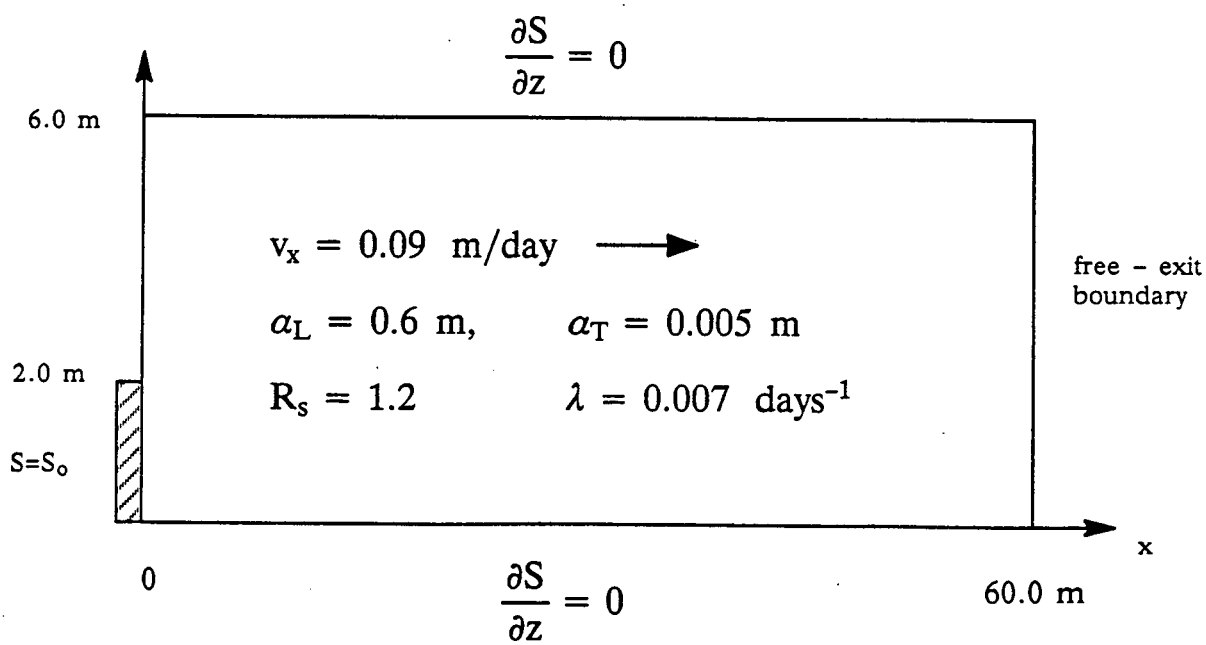

Figure 10. Boundary and transport parameters for numerical and analytical comparison in two-dimensions with one first-order kinetic constant.

Figure 11 compares longitudinal profiles for the analytical and numerical solution at four selected times. Once again, the operator-splitting solution compares very well to the analytical solution in all cases. Figure 12 compares the transverse profiles of the numerical and analytical solutions at three selected times. The results are very encouraging even though there is a small discrepancy near the end of the source (Z = 2.1-2.4 m). Further numerical experimentation (results not shown here) demonstrated that similar differences were found between the nonreactive numerical and analytical solution for the domain shown in Figure 10. Thus, the small differences in Figure 12 are not due to the operator-splitting technique but arise from approximate solution of the nonreactive problem.

Exploring the Possibility of Another ODE Solver

There is a potential criticism of using Runge-Kutta for the solution of the system of reaction equations, namely, that the same amount of work is involved at every node even though there is no reaction occurring in places in the domain where the plume has not reached. One possible approach at overcoming this possible inefficiency is to use another solution technique where the size step is controlled. This is commonly termed "step size control" and is widely of the used as an integral part of many routines that are available to solve systems of ordinary differential equations.

One of the many possible subroutines available for solving systems of ode's has been selected for use. The method is based on the Adam's method where the solution is obtained by replacing the derivative with a polynomial interpolated to computed derivative values followed by integrating the polynomial (Shampine and Gordon, 1975). The routine, DE, uses a given relative and absolute error tolerance, as well as an indicator of the behavior of the derivatives to determine automatically a step size.

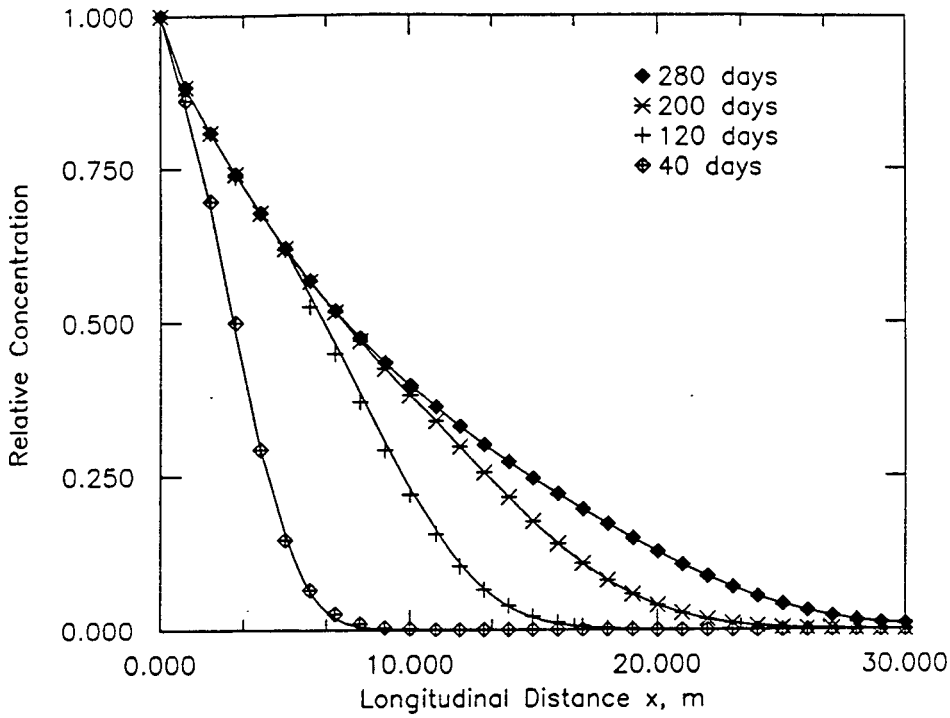

Figure 11. Analytical (lines) and numerical (symbols) comparison of the longitudinal profiles at y = 0 for the two-dimensional case.

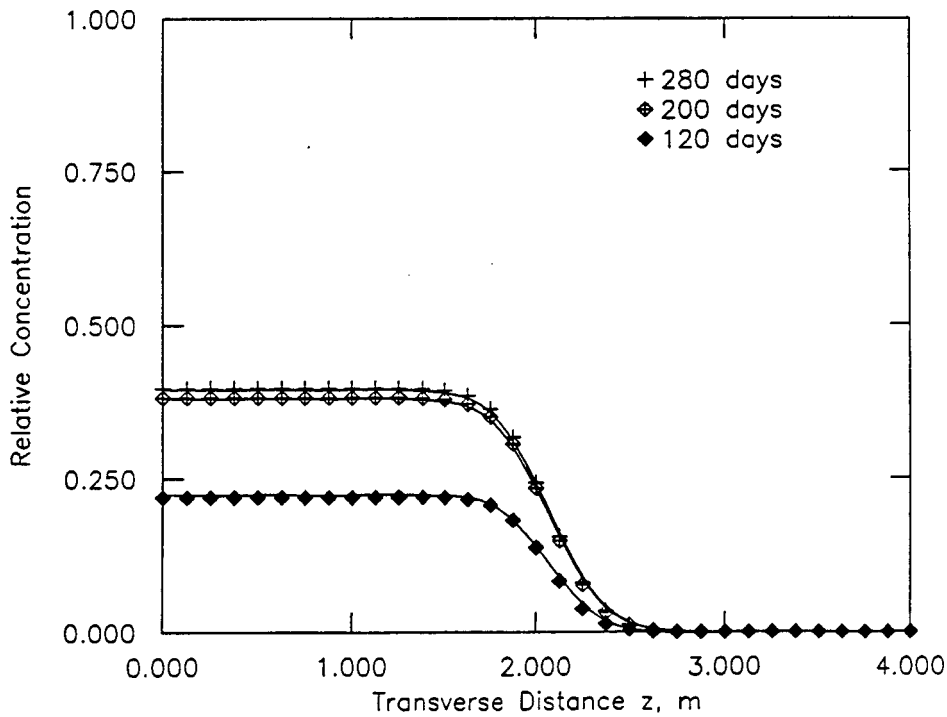

Figure 12. Analytical (lines) and numerical (symbols) comparison of the transverse profiles at x = 10 m for the two-dimensional case.

The DE routine has been implemented into the operator splitting algorithm, and some preliminary work has been done to determine its efficiency and accuracy. Table 3 shows the results obtained thus far, using the exactly same example problem used to examine the Runge-Kutta performance.

Table 3. Performance of the DE Subroutine in the Operator-Splitting Method.

Relative tolerance	Absolute tolerance	Execution time cpu seconds	RSS
0.01	0.01	52.415	0.2296×10^{-6}
0.10	0.10	47.174	0.2306
0.01	0.0001	68.356	0.2293
0.0001	0.01	98.744	0.2291
1.0	1.0	51.034	0.2306

The results are very encouraging that the DE routine can achieve approximately the same accuracy of Runge-Kutta in 47 seconds as opposed to 110 seconds (see Figure 6); however, further evaluation of how the solver is implemented is needed. It is evident from Table 3 that the accuracy of DE is insensitive to the relative and absolute error tolerances for our model problem. It is stressed that these results are subject to further evaluation until the use of DE is considered as a replacement for Runge-Kutta.

Implementation of Biofilm Kinetics

One of the major goals of the modeling research is the analysis of alternative biodegradation submodels. In addition to the dual-Monod submodel, described above, we are implementing the more mechanistically based biofilm model. The overall transport equations will take the form:

Organic

$$\frac{\partial S}{\partial t} = - v_i \frac{\partial S}{\partial x_i} + \frac{\partial}{\partial x_i} D_{ij} \frac{\partial S}{\partial x_j} - R_S ; \quad i,j = 1,2 \tag{4.6}$$

$$R_S = a\, J(S, L_f) \tag{4.7}$$

Acceptor

$$\frac{\partial A}{\partial t} = - v_i \frac{\partial A}{\partial x_i} + \frac{\partial}{\partial x_i} D_{ij} \frac{\partial A}{\partial x_j} - R_A \tag{4.8}$$

$$R_A = \gamma \, a \, J(S, L_f) \tag{4.9}$$

Biomass

$$\frac{\partial (X_f \, L_f)}{\partial t} = R_m \tag{4.10}$$

$$R_m = YJ(S, L_f) - b_T X_f L_f \tag{4.11}$$

where $J(S, L_f)$ = the flux of substrate into the biofilm, a = specific surface area, γ = stoichiometric coefficient, L_f = biofilm thickness, Y = yield coefficient, b_T = total decay, and X_f = biofilm density. The above equation assumes the organic compound is rate-limiting throughout the whole simulation. The flux of substrate into the biofilm is determined using the submodel of Rittmann and McCarty (1981). This submodel is highly nonlinear and involves an iterative Newton-Raphson procedure; details are omitted here. In order to start the simulation an initial biofilm thickness must be assumed.

The biofilm kinetic equations have been implemented into the Runge-Kutta operator-splitting code. This is conceptually straightforward since the only modification required is replacing the dual-Monod equations (e.g., 4.2) by the biofilm equations (e.g., 4.7) on the right-hand-side of the reaction ODEs (e.g., 4.4). The results from the implementation have not yet been verified, however, they appear reasonable numerically. The execution time of a problem similar to the model problem with reaction kinetic parameter typical of denitrification with 10 Runge-Kutta steps was 97.06 seconds. Further work is needed to better characterize the accuracy and efficiency of the biofilm kinetic implementation into the operator-splitting algorithm.

Comparison of Monod and Biofilm Kinetics in a Two-Dimensional Transport Problem

One of the key research questions we are studying is the significance of

using one of the currently available biodegradation models as compared to another. We have designed a numerical experiment to illustrate the differences that can occur when these models are used to describe biological reactions in two-dimensional solute-transport processes.

Figure 13 shows the domain, source location, boundary conditions, and the physical, biological and numerical parameters for the example problem. Monod and biofilm kinetics for the case of single substrate limitation have been chosen as the biological reaction models. The domain and physical parameters shown in Figure 13 are selected from among numerous experiments designed to illustrate the problem at hand. The biological parameters are those obtained for acetate when it was the sole rate-limiting substrate in a denitrying column in experiments discussed by Rittmann et al. (1988). The maximum specific rate of utilization, q_m, was lowered from 2.22 mg SOC/mg cell-day to 0.420 mg SOC/mg cell-day to slow down the kinetics so that important changes that occur can be shown in the selected domain.

The numerical experiments are designed to show the major difference that can occur when external mass transport and internal cell diffusion are included in a biological reaction submodel, i.e., the biofilm model. A continuous source is assumed; also, the same total amount of initial background biomass evenly distributed across the domain is used for both models in order to facilitate model comparison. An initial biofilm thickness of 1 micron was used which roughly corresponds to 0.23 mg/ℓ of attached biomass for use with the Monod model (assuming a film density of 15.0 mg cells/cm^3 and a particle diameter of 1 mm).

The results of the simulations are very interesting and illustrate the difference in the models quite dramatically. The phenomena of interest occurred in a transient fashion and the results are displayed as snapshots of the concentration at selected times. At each time throughout the simulation the

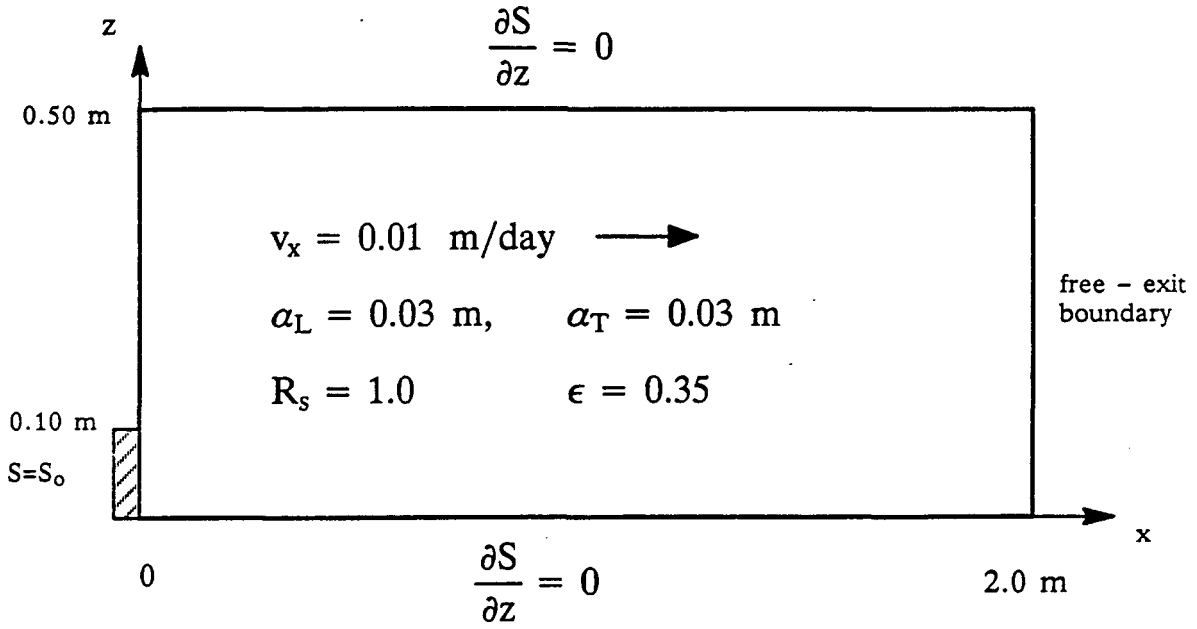

Kinetic Parameters

Monod	Biofilm
q_m = 0.420 mg SOC/mg cell-day	q_m = 0.420 mg SOC/mg cell-day
K = 0.218 mg/L	K = 0.218 mg/L
Y = 0.678 mg cells/mg SOC	Y = 0.678 mg cells/mg SOC
b = 0.07 day $^{-1}$	b = 0.07 day $^{-1}$
	X_f = 15.0 mg cells/cm^3
	D = 1.07 cm^2/day
	D_f = 0.856 cm^2/day
	d_p = 0.10 cm

PDFEM and Operator-Splitting Parameters

Δx = 0.05m	Peclet # = 1.66
Δz = 0.05m	Courant # = 0.10 - 0.20
Δt = 0.5 day 0 - 25days	ϱ_1 and ϱ_2 = 0.06 - .12
Δt = 1.0 day 25 - 250days	Runge - Kutta Steps = 10

Figure 13. Boundary and transport parameters for the rate-limiting compound.

rate-limiting substrate and biomass distribution is constantly changing. The biomass should reach a steady-state when the growth and decay rates are equal.

Figure 14 shows snapshots at 25, 50, 75, and 100 days of the acetate distribution for the Monod reaction submodel. After 25 days the concentration contours resemble the nonreactive case and very little biomass has developed. Not much has happened at this point, biologically speaking. After 50 days, a significant amount of biomass has developed near the source, which can be seen by noticing that the 700 $\mu g/\ell$ contour has shifted almost back to the source location. This indicates there is a very rapid removal near the source and that there is a pinching-off effect of the acetate plume. There will be a nonreactive behaving plume that will result which will never be substantially biodegraded. This pinching-off effect is shown best at the 75 day snapshot. There are clearly two different regimes. The biomass has nearly reached a steady-state at this point (as seen from the biomass mass totals at each time step) and there is very good removal close to the source (notice the 50 ppb contour). It should be clarified that there is some increase in biomass in the middle of the domain, however, not nearly as much as that close to the source. Close to the source the biomass concentration has increased over four orders of magnitude, while there is less than one-order of magnitude increase in concentration in regions away from the source. After 100 days, the pinched-off plume has moved down the domain, advecting and dispersing and slightly biodegrading. The biomass close to the source has now completely reached its steady-state value and is slightly decaying. It is concluded that the biodegradations are quite high to enable such a pinching-off effect and this is reinforced by examining similar, less dramatic behavior with biofilm kinetics. The 200-day contour plot (not shown) shows that the pinched-off plume has almost completely exited the domain and the biomass has decayed further.

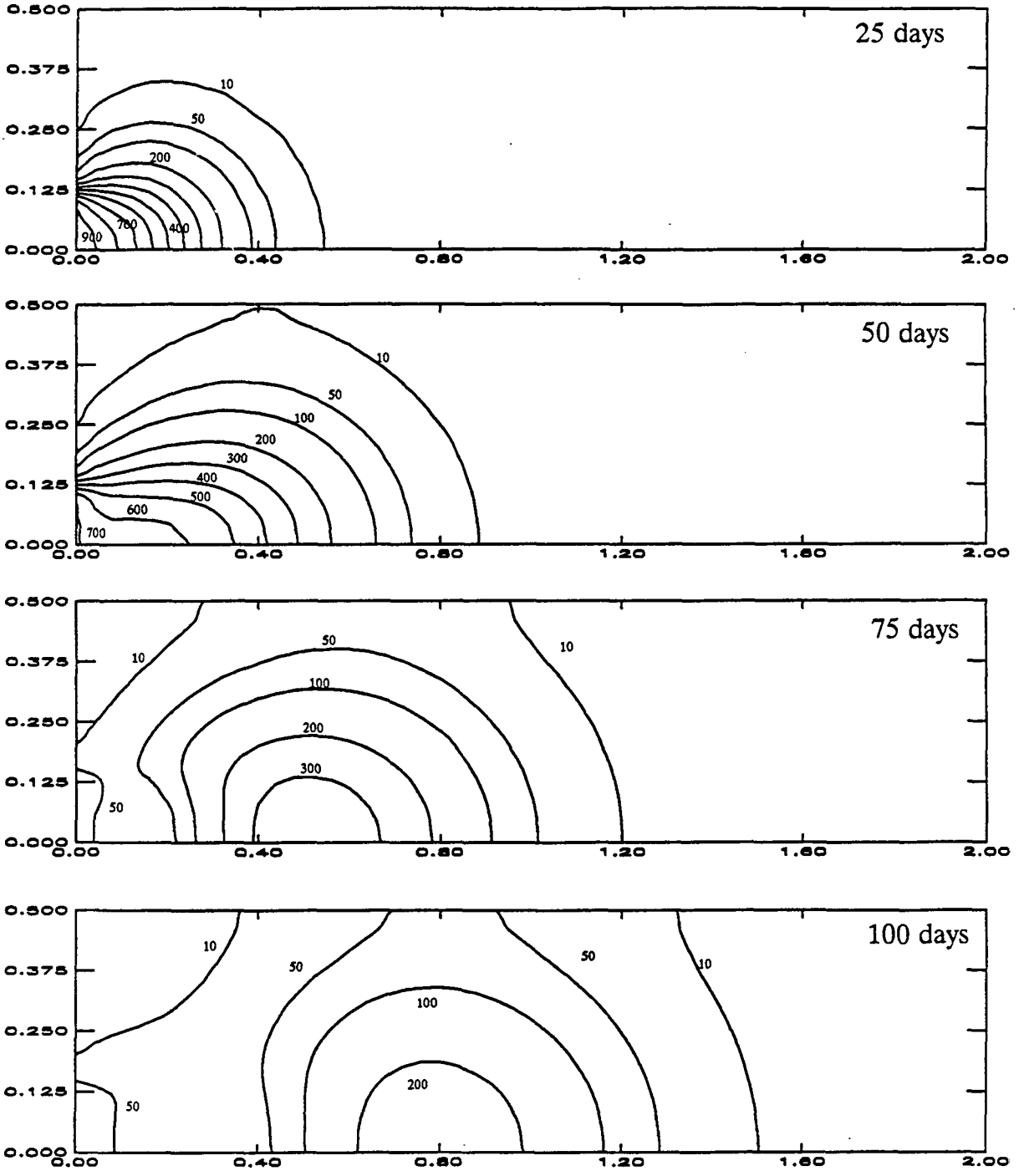

Figure 14. Snapshots of the acetate concentration for Monod reaction (contour values are in μg/L).

Figure 15 illustrates the results for the biofilm submodel which displays much less biodegradation as compared to the Monod case. Only two snapshots are necessary to get the picture of the situation for the biofilm case. The snapshot at 100 days shows that a biofilm is starting to develop as indicated by the developing substrate concentration profile at Z = 0 m and by the biofilm contours (not shown here). It appears that the kinetics are not fast enough to promote the pinching-off effect as seen with the faster Monod kinetics. The snapshot at 200 days indicates the biofilm is nearly at steady-state, which is also confirmed by the biofilm contour plot at 200 days. The total biofilm mass, which was calculated at every time step during the simulation, indicated the biofilm is still growing slightly at 200 days. The Monod biomass on the other hand reached a clear steady-state at approximately 75 days.

The overall conclusion of the numerical experiment is that the Monod kinetics are much faster than biofilm. The reasons are that, in the biofilm model, an external diffusion layer reduces the concentration that drives the biological reaction and that internal diffusion within the biofilm competes with the biological reaction term. Further numerical experiments will focus on the use of dimensionless parameters expressing the relative importance of these processes. In theory, the biofilm model should mimic the Monod model if the parameters are varied such that the effects of external mass transport and internal cell diffusion are minimized.

PNL Research Collaboration

Professor Valocchi and Mr. Odencrantz visited with PNL scientists on November 9 and 10. The major purpose of the trip was to discuss the results from previous tracer experiments performed in the intermediate-scale two-dimensional flow cell, as well as to plan out future experiments. We have obtained all of the existing data and we will work with PNL to interpret the results using

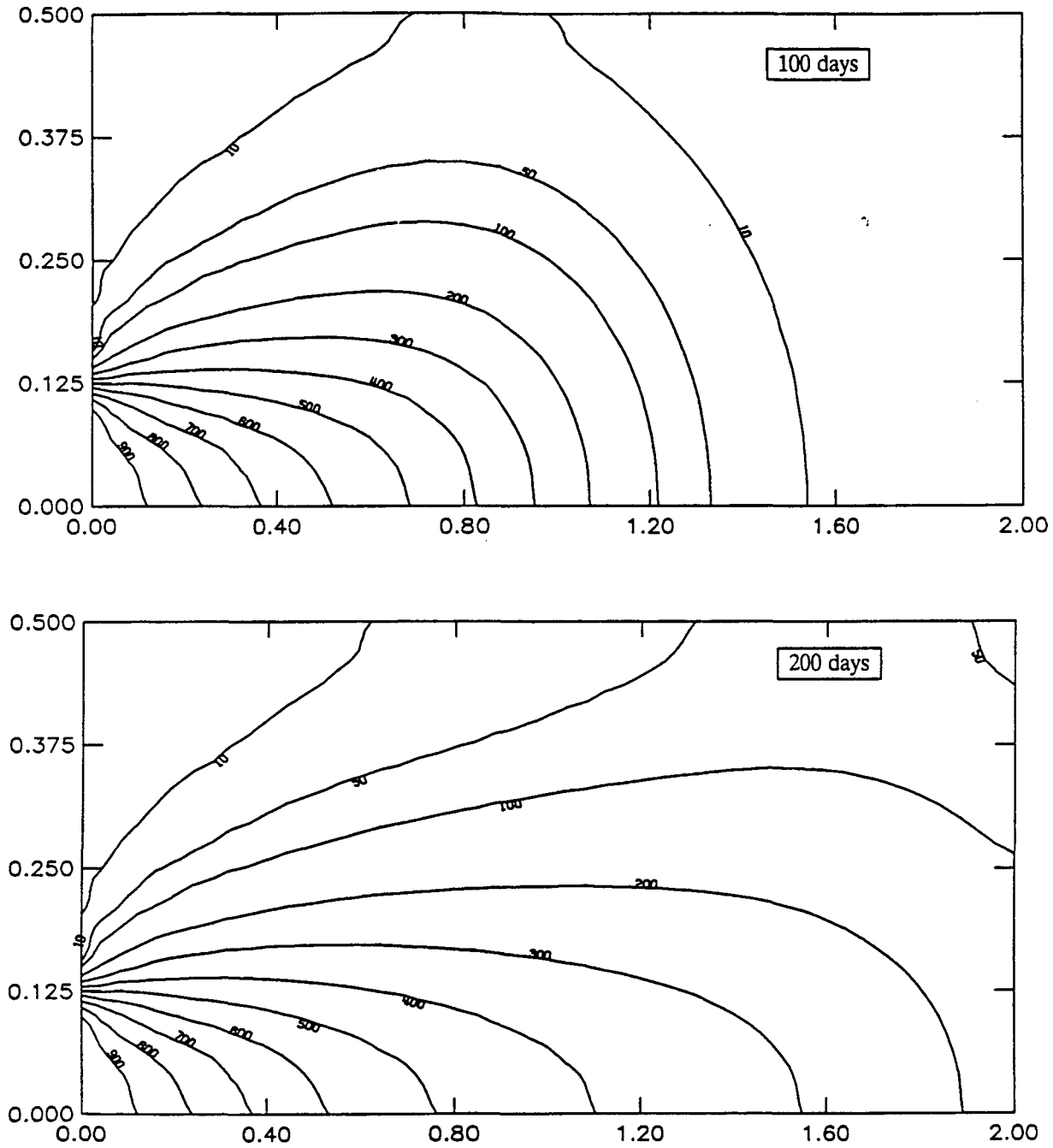

Figure 15. Snapshots of the acetate concentration for biofilm reaction (contour values are in μg/L).

vertically-average, "effective" one-dimensional transport models. PNL plans to conduct another suite of nonreactive tracer studies which we will analyze with our fully two-dimensional model.

In addition to the two-dimensional flow cell experiments, PNL scientists are conducting one-dimensional column experiments with reactive solutes. Of particular interest is a set of biodegradation experiments with quinoline. We also plan to collaborate with PNL on analyzing these results.

Future Directions

(1) A sensitivity analysis will be performed comparing Monod and biofilm kinetics in two-dimensional transport under single-substrate limitation.

(2) We will conduct further numerical experiments which include two substrates (electron donor and acceptor) where either substrate can limit the kinetics depending upon their concentration and kinetic parameters.

(3) Both single and multiple substrate limitation will be studied in a stratified porous medium.

(4) Examination of an initial pulse of mass as opposed to the continuous injection in two-dimensional transport will be conducted.

(5) We plan to continue collaboration with PNL scientists in analyzing the quinoline biodegradation column experiments and two-dimensional tracer experiments.

5. BACTERIAL CLOGGING BY STRICTLY AEROBIC BACTERIA

The principal investigator for this portion of the research is Dr. Philippe Banerge of Cornell University. The research assistants are Philippe Vandervivere and Diego de Lozada. The objective of the research is to determine the mechanisms by which aerobic chemoorganotrophic bacteria clog porous media. Laboratory techniques encompass column percolation studies and direct microscopic

observation via scanning electron microscopy.

Previous Accomplishments

Initial experiments were carried out in a simple sand-column permeameter. The permeameter can be operated with constant head or constant flow rate, although all initial runs were performed with constant head. Piezometers located at the inlet and at 3, 15, and 30 mn from the inlet monitor the pressure loss, including the extra pressure loss due to clogging.

Two bacterial species were chosen. The first is Bacillus subtillis, which is reported to produce large amounts of polysaccharide slime. The second species is Arthrobacter ssp., which are aerobic actinomycetes that grow on gaseous hydrocarbons. Initial experiments were performed with B. subtillis.

A special core sampler was developed for taking small cores (5mm length x 2.5 mm diameter) from the permeameter. These cores can be prepared for scanning electron microscopy directly in the corer. This preparation procedure involves fixation by glutaraldehyde, dehydration by an ethanol series, and critical-point drying. As an alternative, the saturated sand can be prepared by quick freezing in liquid propane, and then sectioned and freeze dried in a Balzers freeze-etching unit.

Clogging results in two experiments showed the sudden onset of clogging. The hydraulic conductivity was reduced to 0.1 to 0.5% of the initial value. Most of the clogging occurred in the first 3 mm.

Scanning electron micrographs showed that B. subtilis grew in head-to-tail chains. No evidence of voluminous extracellular slime was found. Therefore, a preliminary hypothesis was offered: namely, the chains of B. subtillis extend into the pore space and increase the solid surface area which increases the friction factor and tortuosity.

Progress on Bacterial Clogging by Strictly Aerobic Bacteria

Over the past 6 months we have repeatedly modified the design of our experimental setup, and, therefore, the protocol differs from one run to another. We manufactured four plexiglass permeameters to study the effect of strictly aerobic bacteria on the saturated hydraulic conductivity. The experimental setup is shown in Figure 16. As compared to the setup described in the first semi-annual report, the following changes have been adopted. Oxygen concentration in the feed solution is controlled and maintained at a value of 35 mg/l by continuously sparging pure and filter-sterilized oxygen. That precludes the use of a Mariotte bottle (constant head) and therefore we switched to constant flux conditions. The peristaltic pump delivers 1.1 ml/min, which corresponds to a filter-velocity of 0.2 cm/min and a pore-velocity of 0.5 cm/min (7.2 m/day). The safety filter has a pore size of 0.22 microns instead of 0.45 microns. We use Tygon tubing instead of PVC to minimize the losses of dissolved oxygen between the bottle and the permeameter (with Tygon tubing dissolved oxygen drops from 35 mg/l in the bottle to 22-27 mg/l at the permeameter inlet). Three piezometers are inserted in the column at each depth so that channel flow induced by nonuniform clogging can be detected. As shown in Figure 16, they protrude inside the permeameter by 0.3 cm and are located just before the inlet mesh, 0.3 cm, 1.4 cm, 2.5 cm and 3.6 cm downstream of the inlet mesh, with a total of 15 piezometers per permeameter. The saturated hydraulic conductivity can therefore be estimated for a certain region by taking the mean of the three hydraulic head measurements on both sides, calculating the gradient and applying Darcy's law. Between each pair of piezometers (as well as just before and just after the column), a rubber septum was inserted to sample the liquid phase for analysis of dissolved O_2. The mesh that confines the sand inside the permeameter has an opening the size of 50 microns instead of 30 microns.

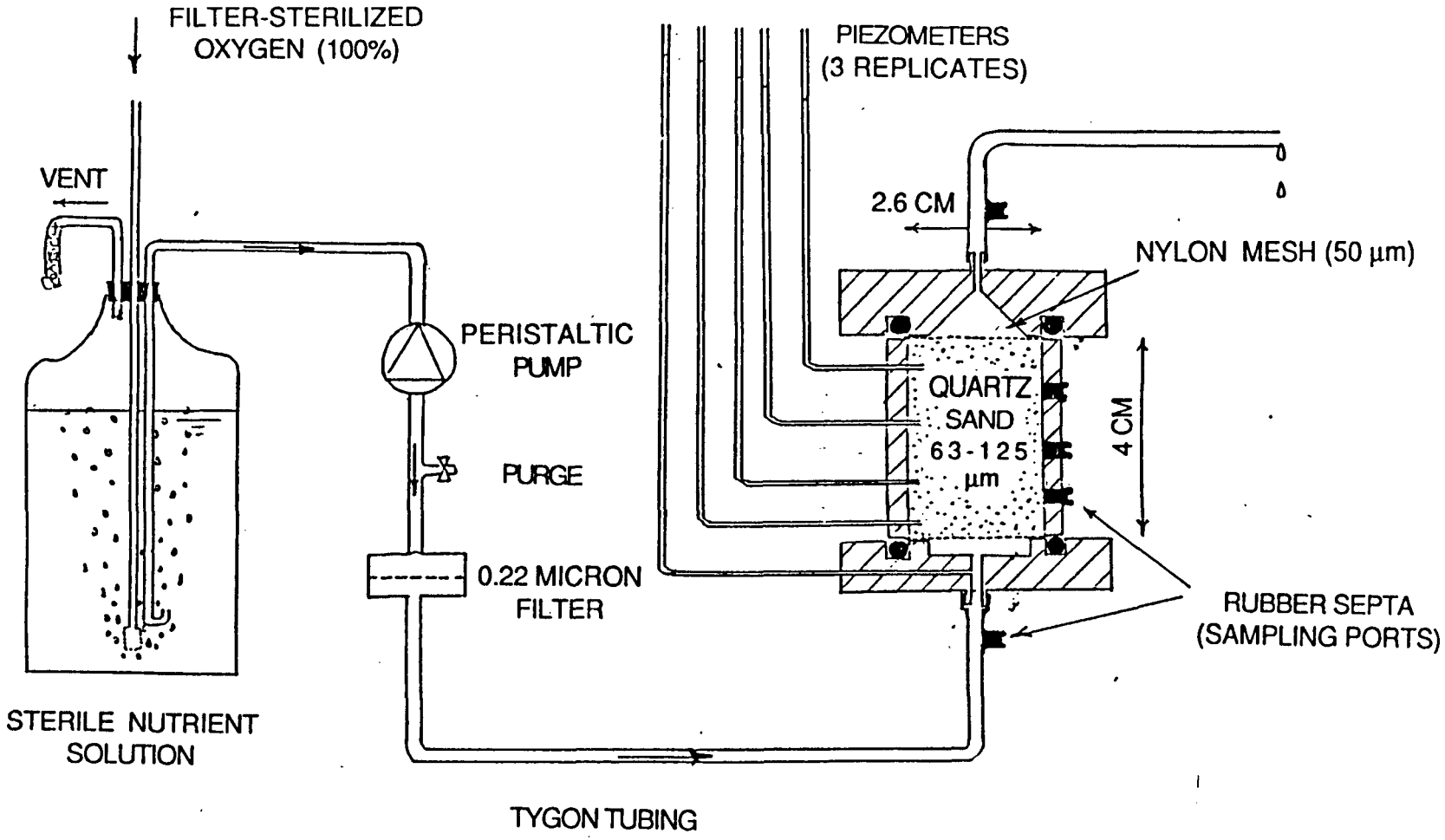

Figure 16. Schematic diagram of constant flux permeameter cells.

The sterilization procedure for the permeameter is much simplified since we have found that an ethylene oxide gas sterilizer (Sybron) is available on campus. The sand column is saturated by gravity and the entrapped air bubbles are eliminated by running the permeameter for 2 days before inoculation.

Several methods were investigated to satisfy the double purpose of distributing the inoculum uniformly throughout the sand column and avoiding the multiplication of the bacteria in the supporting mesh and inlet grooves of the column. We found it satisfactory to inject a large volume (5 ml) of a bacterial suspension diluted to a low cell density (5×10^5 cells/ml) into the permeameter, 0.8 cm downstream of the mesh. This procedure was done without interrupting the flow during or after the injection.

The composition of the nutrient solution has also been modified. First, the glucose concentration was reduced to 100 ppm or less (depending on the treatments) since oxygen availability limits the utilization of more substrate. Secondly, the composition has been changed to allow both organisms used, Bacillus subtilis and Arthrobacter ssp., to be fed with the same defined medium. The medium currently used contains per 1000 ml (in mg): glucose (variable), KNO_3 (30), $MgSO_4 \cdot 7H_2O$ (30), $CaCl_2 \cdot 2H_2O$ (2), $Na_2HPO_4 \cdot 7H_2O$ (165), KH_2PO_4 (80). 0.5 ml of ferric EDTA and 1 ml of trace elements solution. The trace elements solution contained per 1000 ml (in mg): $Al_2(SO_4)3.24\ H_2O$ (35), $SnCl_2 \cdot 2H_2O$ (13), KI (13), $LINO_3$ (13), $MnSO_4 \cdot H_2O$ (20), H_3BO_3 (125), $ZnSO_4 \cdot H_2O$ (25), $Co(NO_3)_2 \cdot 2H_2O$ (25), $CuCl_2 \cdot 2H_2O$ (25), $NiCl_2 \cdot 6H_2O$ (25), $Ba(OH)_2 \cdot 8H_2O$ (13), $Na_2MoO_4 \cdot 2H_2O$ (13), KBr (25). The phosphates and glucose are filter-sterilized and added aseptically to the autoclaved medium.

Both strains used have a minimum doubling time (exponential growth phase) of 4 hours when grown in an agitated flask containing this medium in a more concentrated form at 25°C.

Sampling and preparation for SEM (Scanning Electron Microscopy)

We have developed a technique to prepare and examine absolutely undisturbed samples by SEM. Core-samplers (2 cm in length and 0.6 cm in diameter) are made by rolling a copper sheet (50 microns thick) and soldering the joint. The cylinder can be inserted in the permeameter and retrieved with a sample inside it. The cylinder is connected to the system shown in Figure 17 and washed with a buffer, fixed with glutaraldehyde, dehydrated in an ethanol series, and substituted with a Peldri II-ethanol mixture 1:1. The temperature of the water bath is then raised to 40°C and the sample is infiltrated with pure Peldri II (if the flux driven by gravity is too slow, the inlet can be pressurized with a syringe). The core is subsequently transferred on a cold stage (10°C) to allow the Peldri II to solidify. The sample is then extruded and sectioned with a razor blade. The sections are then transferred in a cold room (4°C) and put under low vacuum to sublimate the Peldri II. Once the sublimation is completed, the samples are mounted, coated with gold and viewed.

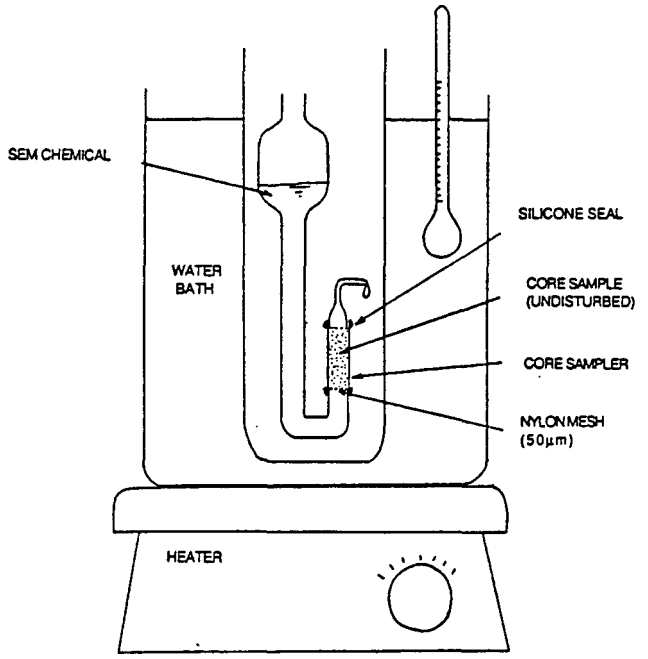

Figure 17. Apparatus used to fix, dehydrate and embed the core samples by infiltration.

Measurement of dissolved oxygen

Samples from the liquid phase of the porous medium are obtained by inserting the needle of a pressure-lock syringe through the septa located along the flowpath in the permeameter. The sand particles are excluded from the sample by insertion of a metal wire through the bore. The needle used is of the "side-port" type to avoid its plugging. It is sterilized by flame. We sample 240 microliters and transfer them in a small glass tube (200 microliters inside volume) whose inside diameter is slightly larger than the electrode tip (3 mm; Microelectrodes Inc.). When tested on an oxygen-free solution, we found that this technique allowed some oxygen to diffuse into the sample, up to 0.6 mg/l, and correction has to be made for this slight experimental error.

Results

The new permeameters were initially tested with a soil isolate (Arthrobacter ssp.) and operated under constant head conditions without any oxygen sparging. We observed an abrupt decrease of the hydraulic conductivity in both permeameters (replicated) (Figures 18 and 19). This reduction occurred solely between the first piezometer, located just before the mesh supporting the sand particles, and the second piezometer, located 3 mm downstream of the mesh. After 5 days, the hydraulic conductivity in the inlet end of the permeameter had dropped by two orders of magnitude in both replicates and after 9 days by three orders of magnitude (Figures 18 and 19). We reported earlier that under similar conditions it took B. subtilis 6 days to cause a reduction of the hydraulic conductivity by two orders of magnitude and at least 20 days in order to cause a reduction by three orders of magnitude.

Interestingly, scanning electron micrographs revealed that the cells colonizing that area were not buried in extracellular polymeric materials coating the sand grains according to the biofilm model but were part of large amassments

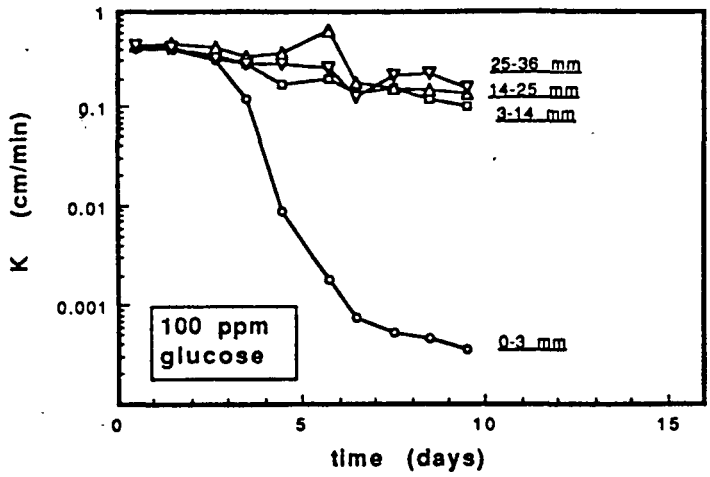

Figure 18. Hydraulic conductivities at different depth intervals in permeameter inoculated with Arthrobacter ssp. and run under constant head conditions.

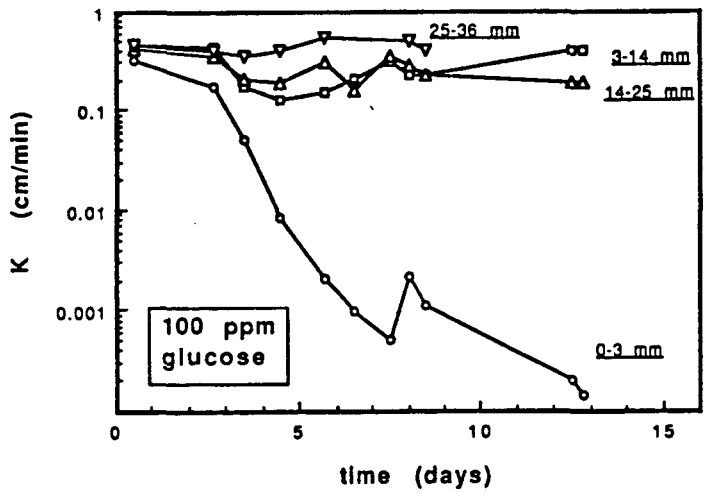

Figure 19. Hydraulic conductivities at different depths intervals in permeameter inoculated with Arthrobacter ssp. and run under constant head until the eighth day and under constant flux thereafter.

apparently trapped at pore necks. Many single cells were sorbed on the solid surfaces but did not produce any extracellular polymers, although they have that property when cultivated in a flask (observation under a light microscope after negative staining with India ink revealed large and loose capsules around the cells). We assembled SEM pictures in order to examine a profile encompassing the first 3 mm of the permeameter and observed a surprisingly low biomass. We therefore suspect that part of the resistance to flow occurred, in fact, upstream of the porous medium in the supporting mesh and in the grooves that distribute the feed solution over the entire section of the mesh. In order to avoid that problem, we decided to inoculate directly inside the permeameter as described previously and hoped that the constant flux conditions would prevent the cells from migrating to the inlet mesh and grooves (Arthrobacter is nonmotile). The results are illustrated in Figures 20 through 23 for different glucose concentrations. At the low glucose concentrations (5-10-20 ppm), the average hydraulic conductivity of the permeameter decreases slowly and reaches a pseudo-steady-state around the tenth day at which time the residual conductivity is 60% and 57% of the initial value for glucose concentrations of 5 and 10 ppm, respectively (Figure 20). At the intermediate glucose concentration (20 ppm), the conductivity decreases slightly more rapidly and never reaches a plateau. At higher glucose concentrations (50-100 ppm), the conductivity decreases much faster and then extremely rapidly to very low values (Figure 20). No steady state occurs at these high glucose concentrations. The exact location of the conductivity reduction is shown in Figures 21, 22 and 23. At the high glucose concentration (100 ppm), clogging develops homogeneously throughout the column for about a week (Figure 23). On the eighth day, clogging stops beyond 1.5 cm and rapidly shifts toward the inlet end as it becomes very severe (on the 12th day the head in the inlet grooves, measured with a mercury manometer, indicated

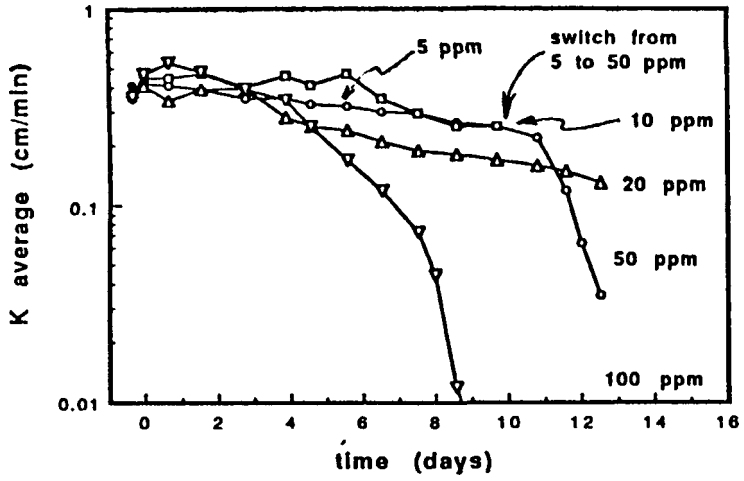

Figure 20

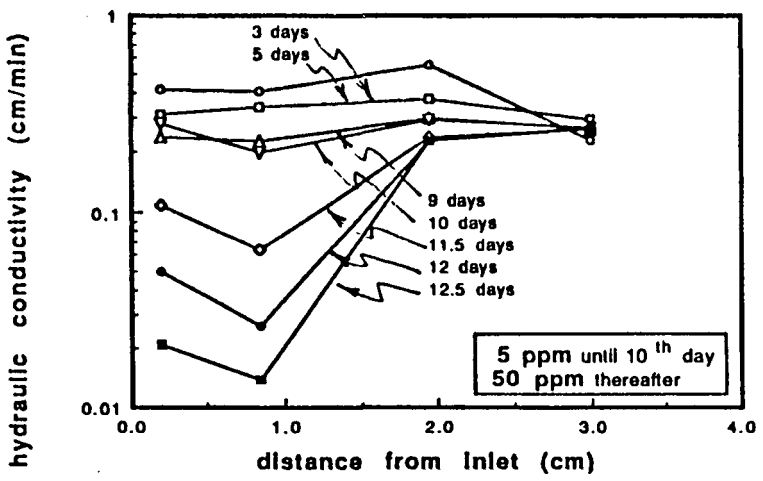

Figure 21

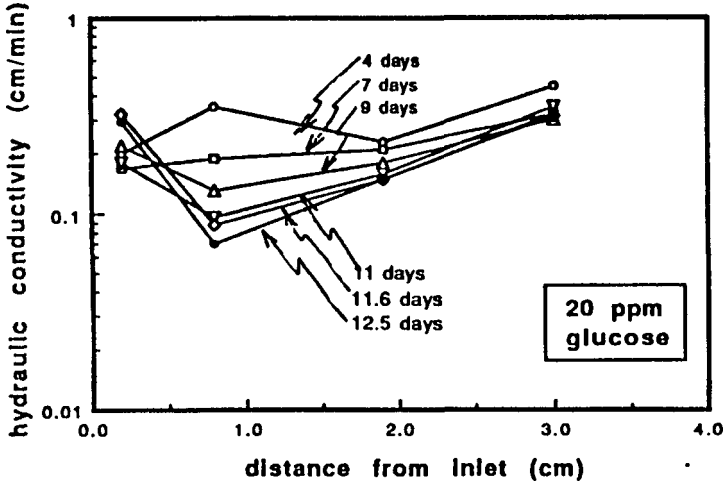

Figure 22

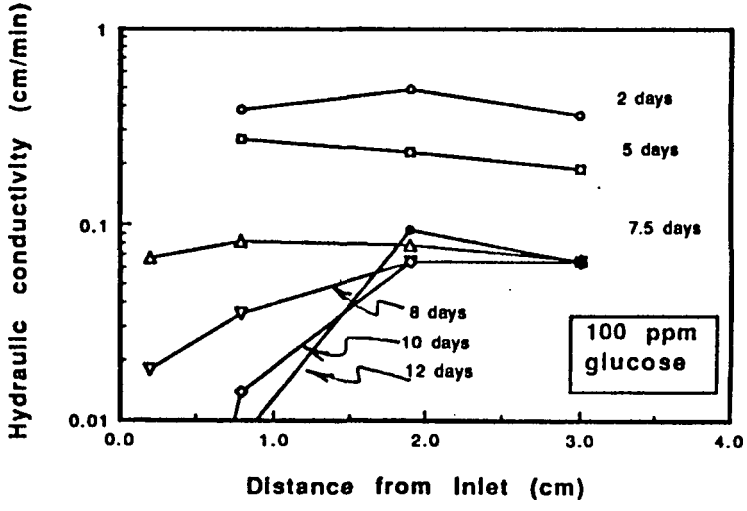

Figure 23

Figure 20. Evolution over time of hydraulic conductivities measured in permeameters inoculated with Arthrobacter ssp and run under constant flux conditions with various concentrations of glucose.

Figures 21-23. Profiles of hydraulic conductivity at different time intervals in permeameters inoculated with Arthrobacter ssp. and run under constant flux conditions with various glucose concentrations.

a reduction of the conductivity of the inlet end by more than 4 orders of magnitude). At the lower glucose concentrations (5-10-20 ppm) clogging never occurs beyond 2.5 cm and is most important between 0.3 and 1.4 cm (Figures 21 and 22).

The profiles showing the evolution of dissolved oxygen inside the permeameters at different time intervals for the different glucose concentrations are illustrated in Figures 24, 25, 26, and 27.

The new permeameters were also tested with B. subtilis under constant flux conditions. We started four permeameters with a combination of two levels of glucose concentration (15 and 100 ppm) and two methods of inoculation (by injection of a small volume-large density inoculum in the feed line or 1 cm downstream the inlet mesh). For each of the 4 permeameters it took approximately 10 days before any reduction could be detected (Figures 28 through 31). Once clogging has started its rate of progress seems to be highly dependent upon the glucose concentration. At low concentration (15 ppm), clogging develops extremely fast (Figures 28 and 29), whereas, at a higher concentration (100 ppm), clogging proceeds much slower (Figures 28 and 31). We wanted to test this interesting observation by switching the glucose concentration from 100 to 15 ppm to see if it would trigger a rapid decrease of conductivity. Unfortunately we had to stop this permeameter right after that and treat it with H_2O_2 because it became accidentally contaminated.

Discussion

We ran permeameters that were inoculated with a pure culture of a soil isolate (Arthrobacter ssp.) and fed with a defined salt medium under both constant head conditions and constant flux conditions. Another important difference between the two sets of experiments was the inoculation method. The constant head permeameters (Figures 18 and 19) were inoculated with a small

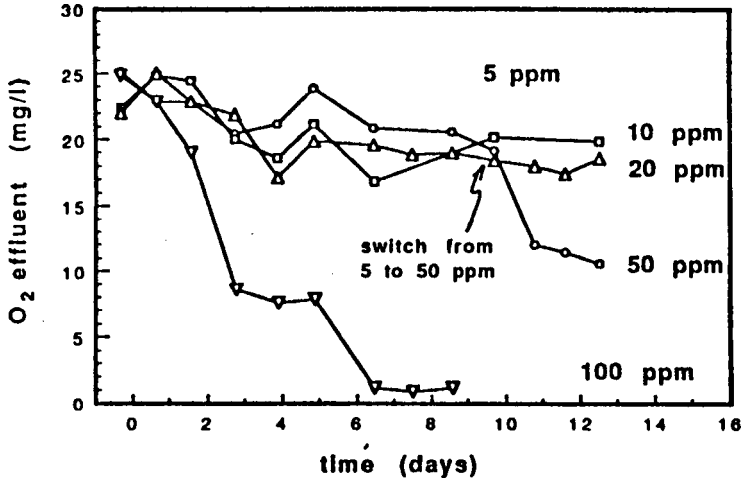

Figure 24

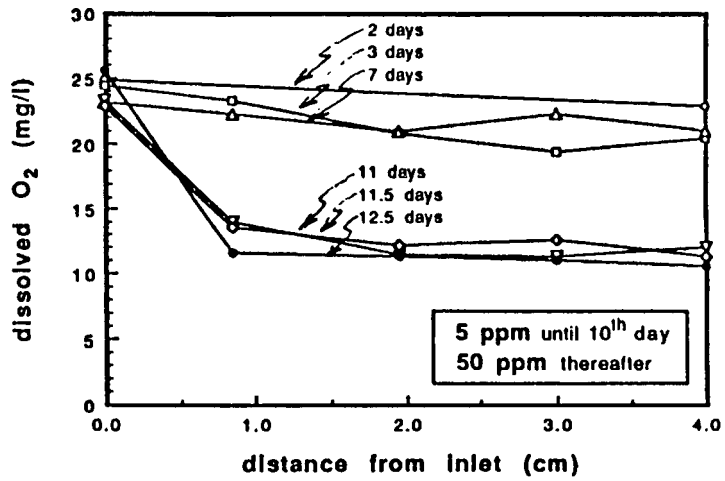

Figure 25

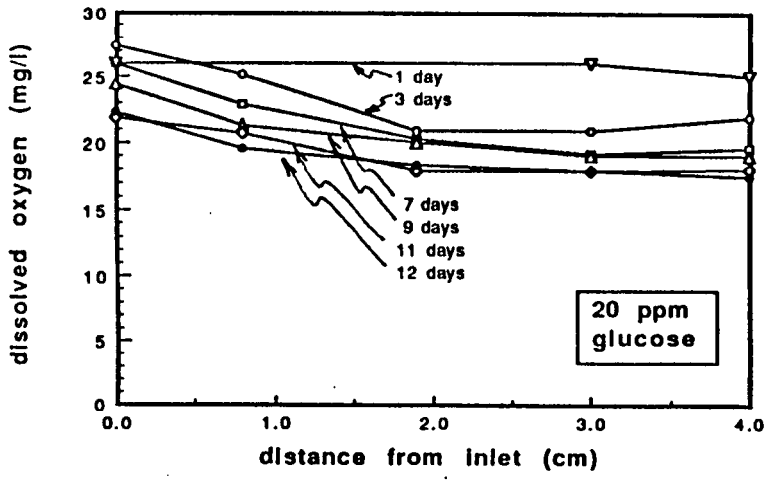

Figure 26

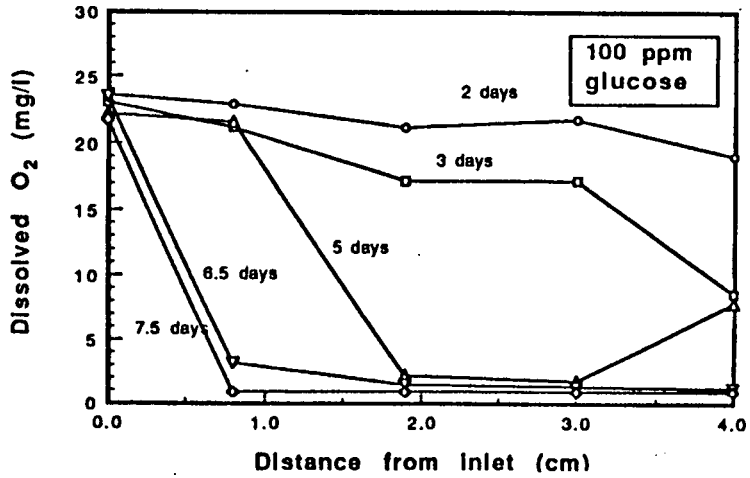

Figure 27

Figure 24. Evolution over time of dissolved oxygen concentration in effluent stream of permeameters inoculated with Arthrobacter ssp. and run under constant flux conditions with various glucose concentrations.

Figures 25-27. Profiles of dissolved oxygen concentration at different time intervals in permeameters inoculated with Arthrobacter ssp. and run under constant flux conditions with various glucose concentrations.

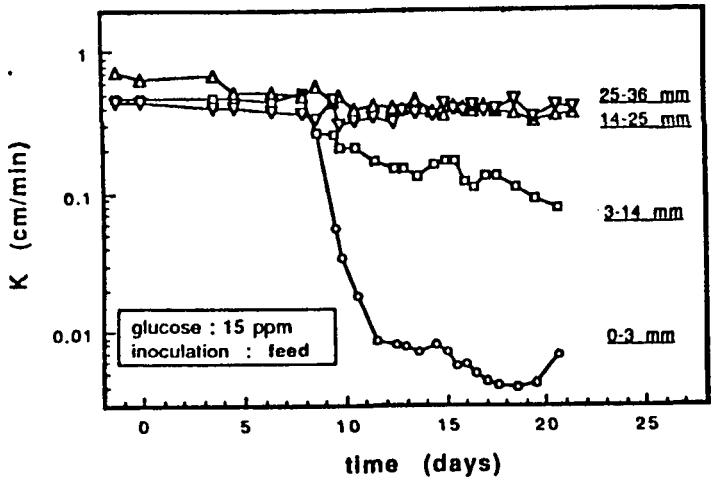

Figure 28

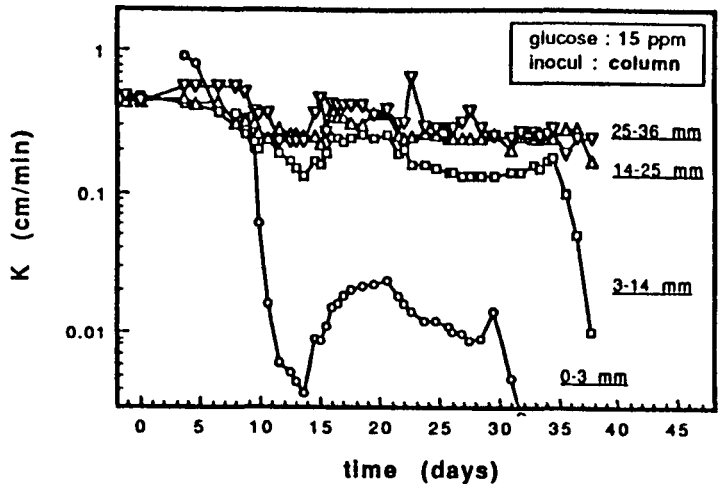

Figure 29

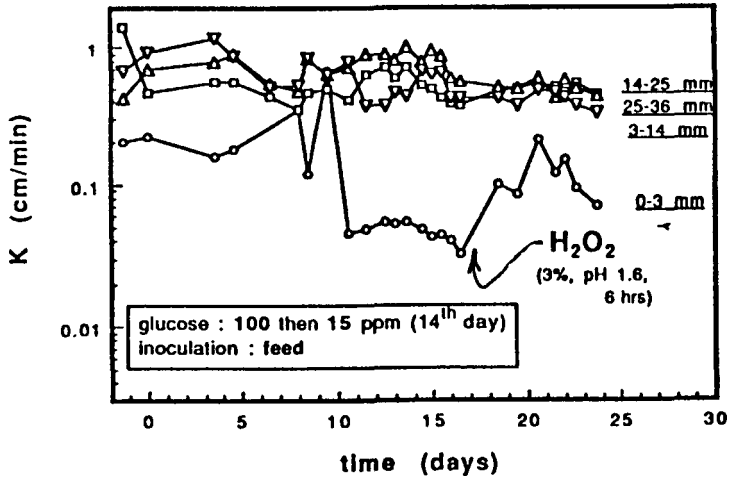

Figure 30

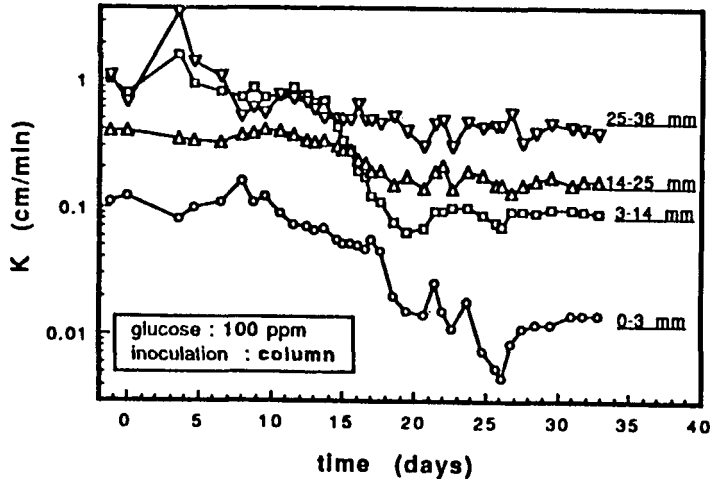

Figure 31

Figures 28-31. Evolution with time of the hydraulic conductivity at different depth increments in permeameters inoculated with Bacillus subtilis and run under constant flux conditions with two levels of glucose concentration and two different techniques of inoculation.

volume (1 ml) of medium cell density (10^6 cells/ml) in the feed line, whereas the permeameters operated under constant flux (Figures 20 to 23) were inoculated with a large volume (5 ml) of smaller cell density (0.5×10^6 cells/ml) directly inside the column, 0.8 cm downstream the inlet mesh. The former permeameters clogged very quickly after the beginning of the experiment to a very low value of conductivity (a decrease of 3 orders of magnitude) but only in the first millimeters of the column. The latter permeameters clogged much deeper, i.e., throughout their length when fed with 100 ppm glucose, only in the first half when fed with 50 or 20 ppm or almost not at all when fed with 10 or 5 ppm. This more diffuse and gradual clogging pattern is probably more representative of what can happen in an actual porous medium. When the hydraulic conductivity drops very sharply, by several orders of magnitude in a matter of days, it always happens at the interface between the porous medium and the body of liquid upstream of it and therefore is not a process related to the porous medium. This hypothesis is based on three observations that can be made when severe clogging develops rapidly, namely, the head loss always occurs before the piezometers that are located at 3 mm depth, SEM pictures reveal surprisingly low cell densities in the first 3 mm of the porous medium, and the inlet grooves become completely filled with biomass. This interface phenomenon is of course emphasized when the inoculum is injected in the feed line (Figures 18 and 19) instead of in the porous medium or when the cells are motile as in the case of B. subtilis (Figures 28 through 31) and therefore can migrate toward the mesh and clog it.

This phenomenon is clearly illustrated by the column fed with 10 ppm glucose. As the cells were restricted to multiply inside the porous medium, conductivity dropped to 56% of the initial value after 10 days of percolation (Figure 20). At that time, some cells accidentally sedimented in the inlet cap (the flow had to be stopped for several hours) and had completely filled up the

inlet grooves after 2 days thereby decreasing the hydraulic conductivity by 2 orders of magnitude (not shown).

Our conclusion is that the decrease of the hydraulic conductivity by two orders of magnitude and more that we observed can occur very rapidly when the cells can easily form a confluent mat as is the case at the inlet end of the permeameter. We never observed, nor to our knowledge has it been ever reported, a decrease of the hydraulic conductivity inside the porous medium, at the exclusion of the inlet interface, by more than 2 orders of magnitude. These mats are typically very thin but very active since they can deplete the oxygen content (25 mg/l) (see Figure 32) and probably the 100 mg/l glucose (see below) of the nutrient solution, which takes less than one minute to flow across the mat.

Why does the hydraulic conductivity stay constant at the initial value in the second half of the permeameters fed with 50 ppm glucose or less (Figures 21 and 22)? The lack of activity of the aerobic bacteria in this region, as indicated by the flat O_2 profiles (Figures 25 and 26), could be caused by the exhaustion of the glucose or by the formation of an unfavorable chemical environment due to the microbial activity in the first half of the permeameter.

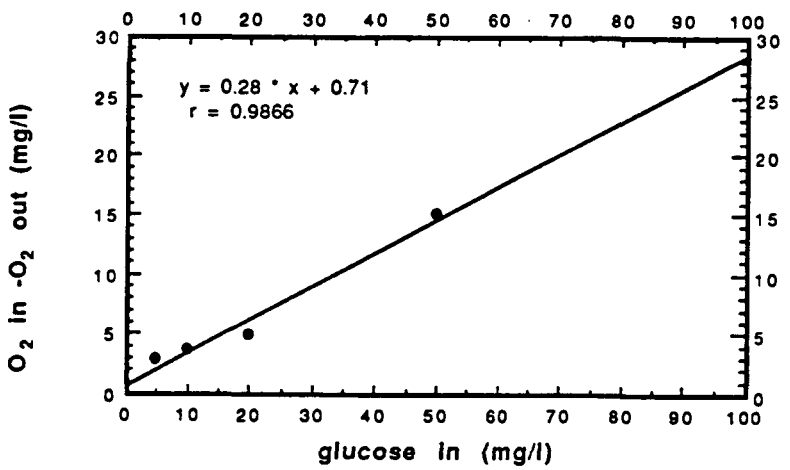

Figure 32. Relationship between the O_2 consumed in the permeameters and the glucose concentration in the feed line.

If the former alternative is true, then it would indicate a glucose consumption to oxygen consumption ratio of 3.6. This is most likely the case since this ratio is constant for the glucose concentrations up to 50 ppm (Figure 32). Indeed, this figure indicates that, except for the run with the 100 mg/l feed, glucose is the nutrient limiting growth and the cells use the oxygen and other nutrients run out of glucose. At the 50 ppm concentration, reduction of the hydraulic conductivity to 2.5% of the initial value (Figure 21) occurred in a completely aerobic system. Given a ratio of glucose to oxygen consumption of 3.6, the O_2 requirement to fully oxidize the 100 mg/l of glucose amounts to 28 mg/l which is slightly more than provided in the feed. After 7.5 days of percolation, the column supplied with 100 mg/l glucose became depleted in O_2 beyond 0.8 cm (Figure 27) which correlates well with the inhibition of further clogging beyond this point (Figure 23).

The O_2 profile at day 5 in Figure 27 may seem surprising since the O_2 concentration rises from 1.7 at 3 cm depth to 7.8 mg/l in the effluent. In fact, the liquid sampled at depths 1.9 and 3 cm were probably coming from zones with no flow that are bypassed by the oxygenated solution. We are aware of that because the samples came from areas close to piezometers having a head nearly identical to the effluent head and much lower than the head of the other piezometers at the same depth. This is an indication that clogging does not happen uniformly in a plane perpendicular to the general direction of flow and that channel flow must occur to a large extent, thereby increasing the dispersivity of the porous medium.

We shall discuss only briefly the results of the runs under constant flux with B. subtilis (Figures 28 through 31) because the SEM analysis revealed the presence of contaminating microorganisms that must have affected the results during the latest stages of the experiments. We hope that the new sterilization

technique will decrease the probability of such contaminations. The two inoculation techniques tested do not seem to affect the clogging, which is actually not surprising given that our strain is motile. Compared to the results presented in our first semi-annual report, the data shown here are characterized by a longer initial lag phase during which the conductivity is constant and by a less severe reduction of the conductivity. Moreover, the bacteria that were visible on electron micrographs did not form long chains of cells attached in a tail-to-head fashion and extending through the pore space, but were disseminated in the porous medium as small sorbed colonies. This different colony morphology might be the result of the mixed culture (contaminants) or of the different composition of the nutrient medium. It should be noted that the preparation of the specimen with Peldri II as a drying agent was of outstanding quality.

Conclusions

Both aerobic strains tested can decrease the hydraulic conductivity of the sand column under constant flux conditions by several orders of magnitude without excretion of exopolymers and without biofilm formation. It is observed that when the bacteria reach and start colonizing the restraining wire mesh and the chamber at the inlet end of the permeameter, a dense bacterial mat is rapidly formed. This mat seems to present a high resistance to flow even when the feed solution has a low glucose concentration. On the other hand, when the cells are restricted to multiply exclusively inside the porous medium, they clog the permeameter much deeper and at a much slower pace even at higher substrate concentrations.

Future work

The next two steps, in the short term, consist in developing a sensitive technique to measure biomass profiles in the permeameters (probably phospholipids

assay), and secondly to conduct experiments with mixed cultures of subsurface isolates.

Progress on Bacterial clogging by methanogenic bacteria

Research was initiated in September on the mechanisms involved in the clogging of porous media by methanogenic bacteria. One reason for our interest in methanogens is that, since the result of their metabolism is the production of a relatively insoluble gas, their study allows the consideration of one additional clogging mechanism compared with strictly aerobic bacteria, namely, gas entrapment resulting from bubble formation.

We are currently designing and building a particular type of permeameter, modified from that used in the experiments with aerobic bacteria, that would allow us to collect the gas exiting the column and to determine the volume of the methane bubbles entrapped within the sand column. The first experiments will be carried out under constant-head conditions, with the possibility of moving eventually to constant flux in subsequent runs. The experiments will be conducted under anoxic conditions. To maintain these conditions over time, the air access tube of the Mariotte bottles and the piezometers will be opened to a nitrogen environment at atmospheric pressure.

6. REFERENCES

Cartier, P.H. 1968. "Dosage des pyridine nucleotides oxides et reduits dans le sang et les tissus animaux." European J. Biochem., 4, 247-255.

Cheer, S., Gentile, J.H. and Hegre, C.S. 1974. "Improved methods for ATP analysis." Anal. Biochem., 60, 102-114.

Claus, D. and Walker, N. 1964. "The decomposition of toluene by soil bacteria." J. Gen. Microbiol., 36, 1, 107-122.

Drew, S.W. 1981. "Liquid culture." Manual of Methods for General Bacteriology. P. Gerhardt (ed.-in-chief). American Society for Microbiology, Washington, DC.

Freeze, R.A. and Cherry, J.A. 1979. Groundwater. Prentice-Hall, Inc., Englewood Cliffs, NJ.

Fried, J.J., Muntzer, P. and Zilliox, L. 1979. "Ground-water pollution by transfer of oil hydrocarbons." Groundwater, 17, 6, 586-594.

Frind, E.O. 1988. "Solution of the Advection-Dispersion Equation with Free Exit Boundary." Numerical Methods for Partial Differential Equations, 4, 301-313.

Gillham, R.W. and Cherry, J.A. 1982. "Contaminant migration in saturated unconsolidated geologic deposits." Recent Trends in Hydrogeology, Geologic Society of America Special Paper 189. T.N. Narasimhan (ed.). The Geological Society of America, Boulder, CO.

Harrison, D.E.F., MacLennan, D.C. and Pirt, S.J. 1969. "Response of bacteria to dissolved oxygen tension." In Fermentation Advances, D. Perlman (ed.), Academic Press, London, pp. 117-144.

Hess, H.H. and Derr, J.E. 1975. "Assay of inorganic and organic phosphorus in the 0.1-5 nanomole range," Analyt. Biochem., 63, 607-613.

Holm-Hansen, O. and Karl, D.M. 1978. "Biomass and adenylate energy charge determination in microbial cell extracts and environmental samples." In Methods in Enzymology, Vol. LVII. Bioluminescence and Chemiluminescence. M.L. DeLuca (ed.). Academic Press, 73-85.

Hunt, J.R., Sitar, N. and Udell, K.S. 1988. "Nonaqueous phase liquid transport and cleanup. I. Analysis of mechanisms." Water Resources Research, 24, 8, 1247-1256.

Lanzetta, P.A., Alvarez, L.J., Reinach, P.S. and Candia, O.A. 1979. "An improved assay for nanomole amounts of inorganic phosphate." Anal. Biochem., 100, 95-97.

MacQuarrie, K.T.B., Sudicky, E.A., and Frind, E.O. 1989. "Simulation of biodegradable organic contaminants in groundwater 1. Numerical formulation and model calibration." Water Resour. Res., in press.

Mallette, M.F. 1969. "Evaluation of growth by physical and chemical means." Methods in Microbiology, Vol. 1, J.R. Nomis and D.W. Ribbons, eds., Academic Press, London.

Matin, A. and Gottschal, J.C. 1976. "Influence of dilution rate on NAD(P) and NAD(P)H concentrations and ratios in a Pseudomonas sp. grown in continuous culture." J. Gen. Microbiol., 94, 333-341.

Rittmann, B.E. and P.L. McCarty. 1981. "Substrate Flux into Biofilms of Any Thickness." J. Environ. Eng., 107: 831-849.

Rosenberg, M., Gutnick, D. and Rosenberg, E. 1980. "Adherence of bacteria to hydrocarbons: A simple method for measuring cell surface hydrophobicity." FEMS Microbiology Letters, 9, 1, 29-33.

Sáez, P.B. and Rittmann, B.E. 1989. "Discussion of Kinetics and Stoichiometry of Activated Sludge Treatment of Toxic Organic Wastewater." J. WPCF, 61, 357-358.

Shampine, L.F. and M.K. Gordon. 1975. "Computer Solution of Ordinary Differential Equations." W.H. Freeman and Company, San Francisco.

Vershueren, K. 1983. Handbook of Environmental Data on Organic Chemicals, 2nd edition. Van Nostrand Reinhold Co., New York.

Welty, J.R., Wicks, C.E. and Wilson, R.E. 1984. Fundamentals of Momentum, Heat, and Mass Transfer, 3rd edition. John Wiley & Sons, New York.

Wheeler, M.F. 1988. "Modeling of highly advective flow problems." In Developments in Water Science, Vol. 1, Modeling Surface and Sub-Surface Flows, Elsevier, pp. 35-44.

Wheeler, M.F., and Dawson, C.N. 1987. An Operator-Splitting Method for Advection-Diffusion-Reaction Problems. Department of Mathematical Sciences, Rice University, Technical Report 87-9.

Wilson, D.F., Erecinska, M., Drown, C. and Silver, I.A. 1977. "Effect of oxygen tension on cellular energetics." Am. J. Physiol., 233, C135-C140.

Wimpenny, J.W.T. and Firth, A. 1972. "Levels of nicotinamide adenine dinucleotide and reduced nicotinamide adenine dinucleotide in facultative bacteria and the effect of oxygen." J. Bacteriol., 111, 24-32.